Atmospheric Research 284 (2023) 106606

Contents lists available at ScienceDirect

Atmospheric Research

journal homepage: www.elsevier.com/locate/atmosres

Evaluation of ERA5 and ERA5-Land reanalysis precipitation datasets over Spain (1951–2020)

José Gomis-Cebolla [a,*], Viera Rattayova [b], Sergio Salazar-Galán [a], Félix Francés [a]

[a] Research Institute of Water and Environmental Engineering, Universitat Politècnica de València, Valencia 46022, Spain
[b] Slovak University of Technology, Department of Land and Water Resources Management, Radlinského 11, 810 05, Bratislava 1, Slovakia

ARTICLE INFO

Keywords:
Reanalysis precipitation
AEMET
ECMWF
Continuous/categorical/pdf assessment
Spatial pattern
Temporal trend

ABSTRACT

Reanalysis precipitation estimates are widely used in the fields of meteorology and hydrology because they can provide physical, spatial, and temporal coherent long time series at a global scale. Nevertheless, as a pre-requisite for many applications their performance needs to be assessed. The objective of this study was to evaluate the European Centre for Medium-Range Weather Forecasts (ECMWF) latest fifth-generation reanalysis precipitation products, i.e., ERA5 and ERA5-Land, at country scale in Spain. For doing so, we compared it against a high-resolution precipitation product of the Spanish Meteorological Agency which spans approximately 70 years (1951–2020). A comprehensive assessment (continuous, categorical, probability distribution function (pdf), spatial pattern, and temporal trend) was performed in order to ascertain the quality of the reanalysis products. Results of the analysis revealed a general agreement between observations and ERA5-Land/ERA5 estimates: spearman correlation values between 0.5 and 0.9, Root Mean Square Error (RMSE) mostly between 2 and 8 mm/d and Kling Gupta Efficiency (KGE) values >0.4. Categorical assessment additionally indicated a good performance (Heiken Skill score (HSS) score, also known as kappa, between 0.4 and 0.8). Nevertheless, performance was found to be dependent on the climatic region, precipitation intensity and orography. Correlation revealed a north-west (higher values) south-east (lower values) spatial gradient while relative bias (RBIAS) and RMSE spatial patterns were positively correlated with slope ($\rho = 0.41/0.35$, $0.69/0.70$, respectively). In addition, as indicated by the categorical analysis, along the Mediterranean coast a wet bias (i.e., overestimation of days with precipitation) was found. Reanalysis detection capacity (kappa) shown a negative correlation with the slope ($\rho = -0.29/-0.34$). Worst model performance is obtained during summer months, with a generalized overestimation. The pdf assessment revealed that the ERA5-Land/ERA5 tended to overestimate light ($\geq$1 and $<$ 5 mm/day), and moderate ($\geq$5 and $<$ 20 mm/day) precipitation categories while underestimating the heavy ($\geq$20 and $<$ 40 mm/day) and violent ($\geq$40 mm/day) categories. Moderate precipitation provided the best detection capacity, as indicated by the precipitation-intensity analysis. ERA5-Land/ERA5 showed a good capacity to reproduce the spatial patterns and temporal trends of the observations. ERA5-Land and ERA5, with a different spatial resolution, performed very similar in all the analysis considered. Mediterranean and northern coast were highlighted as the most critical for reanalysis modelling purposes because of its performance.

1. Introduction

Reliable and accurate precipitation information of fine spatio-temporal resolution is of paramount importance for many applications in the fields of hydrology, meteorology, climatology, natural hazards management, and human activities (Ebert et al., 2007; Piao et al., 2010; Robertson et al., 2013; He et al., 2020; Salazar-Galán et al., 2021). Nevertheless, the spatial estimation of this variable is challenging both because of its spatio-temporal heterogeneity and the diverse physical processes involved (Tapiador et al., 2012; Nogueira, 2020).

Atmospheric reanalysis result from the combination of observations from multiple variables and numerical weather forecasts using data assimilation methods (Hu et al., 2019). They can provide physical, spatial, and temporal coherent continuous long records of multiple climate variables, including precipitation (Sun et al., 2018; Hu et al., 2019). Thus, they can be considered a potential alternative to ground-based observations especially in ungauged or poor-gauged regions (Amjad et al., 2020).

* Corresponding author.
E-mail address: jgomceb@iiama.upv.es (J. Gomis-Cebolla).

https://doi.org/10.1016/j.atmosres.2023.106606
Received 3 August 2022; Received in revised form 21 December 2022; Accepted 2 January 2023
Available online 4 January 2023

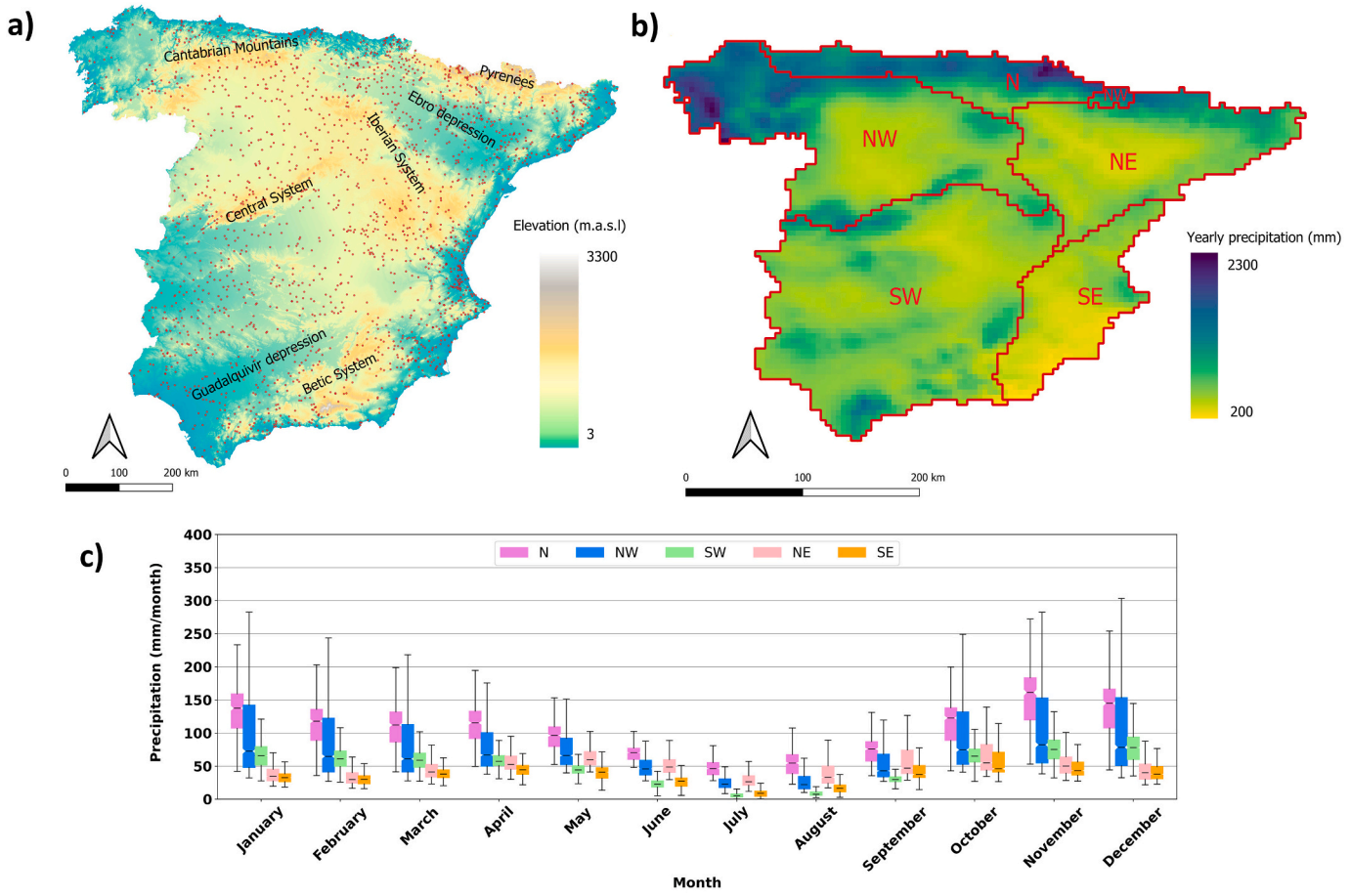

Fig. 1. Digital elevation model of continental Spain and spatial distribution of observations (a). Mean yearly precipitation (1951–2020) together with the climatic regions considered in this study (b). Monthly temporal evolution (c).

Table 1
Overview of the precipitation datasets used in this study.

Name	Details	Spatial resolution	Time resolution	Reference
AEMET	Gridded	0.05° x 0.05°	1 d	Peral García et al., 2017
ERA5	Reanalysis	0.25° x 0.25°	1 h	Hersbach et al., 2020
ERA5-Land	Reanalysis	0.10° x 0.10°	1 h	Muñoz-Sabater et al., 2021

In the last few years, significant progress has been made in the development of global reanalysis systems. The National Center for Environment Prediction/National Center for Atmospheric Research (NCEP/NCAR) released the NCEP1 (Kalnay et al., 1996) and NCEP2 (Kanamitsu et al., 2002) with a spatial resolution of 2.5°x2.5° and 1.875°x1.875°, respectively. The National Aeronautics and Space Administration (NASA) Global Modelling and Assimilation Office (GMAO) released the MERRA reanalysis (Rienecker et al., 2011), which was replaced by the MERRA-2 (Gelaro et al., 2017), both at a resolution of 0.5°x0.67°. The Japanese Meteorological Agency (JMA) provided the Japanese 55-year Reanalysis (JRA-55; Ebita et al., 2011) with 1.25°x1.25° spatial resolution and overcame the deficiencies of the first reanalysis project. The European Centre for Medium-Range Weather Forecast (ECMWF) released several reanalysis products: ERA-15 (Gibson et al., 1999), ERA-40 (Uppala et al., 2005), ERA-Interim (Dee et al., 2011), and recently, the fifth generation, i.e., ERA5 (Hersbach et al., 2020) followed by ERA5-Land (Muñoz-Sabater et al., 2021). They feature temporal and spatial resolution easily competitive with satellite-based precipitation estimates (Muñoz-Sabater et al., 2021). These two come at 1 h temporal resolution and 0.25°x0.25° and 0.1°x0.1° spatial resolution, respectively.

Reanalysis are influenced by both model and observations errors (Bosilovich et al., 2008). In addition, model performance can be influenced also by orography incorrectness, data assimilation and parametrization of small-scale processes (Bližňák et al., 2022). Comprehensive evaluation of reanalysis precipitation thus becomes essential prior to any further use and many studies have been devoted to the evaluation of these datasets at global and regional levels. Amongst the different agencies' reanalysis products, ERA-Interim has been generally considered to provide the best performance in precipitation estimation (Beck et al., 2017, 2019; Wang et al., 2019). Recent studies conclude that in fact, new ECMWF releases (i.e., ERA5 and ERA5-Land) outperform its predecessor ERA-Interim (Beck et al., 2019; Amjad et al., 2020; Gleixner et al., 2020; Hamm et al., 2020; Nogueira, 2020). The evaluation of these ECMWF products considering national/regional networks or under a hydrological modelling framework highlighted that ERA5 and ERA5-Land estimates are not free from associated uncertainties (Beck et al., 2019; Sharifi et al., 2019; Amjad et al., 2020; Kolluru et al., 2020; Tang et al., 2020; Tarek et al., 2020; Bandhauer et al., 2022; Hafizi and Sorman, 2022; Xu et al., 2022). Despite its capability of capturing precipitation events and reproducing the spatio-temporal distribution of this variable, biases are reported in most analyses and performance is also affected by complex orography.

In Spain country, precipitation features a high spatial and temporal variability because of a complex orography and diverse atmospheric regimes (Serrano et al., 1999) influenced by both Atlantic and

Table 2
Statistics metrics used in the continuous, categorical and spatial pattern assessment. x_i and y_i refers to AEMET and ERA reanalysis respectively. n represents the total number of points. μ refers to the mean value and σ to the standard deviation. $I(k)$ and $J(k)$ are the time steps when the kth largest values occur. For SPAEF, sp. subindex indicates the calculation is performed using spatial values. K and L refers to the given histogram of AEMET and ERA spatial patterns, which has been discretized into p thresholds. RMSE is given in mm/day, mm/month or mm/year depending on the timestep considered.

Metric	Expression	Optimal [min,max] value	Unit
Spearman correlation	$\rho = 1 - \frac{6\sum (x_i - y_i)^2}{n(n^2-1)}$	1, [−1,1]	–
RBIAS	$RBIAS = \frac{\sum (x_i - y_i)\cdot 100}{\sum (x_i)}$	0, (−∞,∞)	%
RMSE	$RMSE = \sqrt{(1/n)\sum (x_i - y_i)^2}$	0, [0, ∞)	mm/timestep
KGE	$KGE = 1 - \sqrt{(\rho-1)^2 + (\alpha-1)^2 + (\beta-1)^2}$ $\alpha = 1 - 1/2\left(\sum \left\lvert \frac{y(I(k))}{n\mu_y} - \frac{x(J(k))}{n\mu_x} \right\rvert\right)$ $\beta = \mu_y/\mu_x$	1, (−∞, 1]	–
POD	$POD = H/(H+M)$	1 [0,1]	–
FAR	$FAR = F/(H+F)$	0, [0,1]	–
HSS(κ)	$HSS = 2(HCN - FM)/[(H+M)(M+\mathrm{CN}) + (H+F)(F+\mathrm{CN})]$	1, [−1,1]	–
SPAEF	$SPAEF = 1 - \sqrt{(\rho_{sp}-1)^2 + (\alpha_{sp}-1)^2 + (\beta_{sp}-1)^2}$ $\alpha_{sp} = \sum_{j=1}^{p} min(K_j, L_j) / \sum_{j=1}^{p} K_j$ $\beta_{sp} = (\sigma_y/\mu_y)/(\sigma_x/\mu_x)$	1, (−∞, 1]	–

Table 3
Confusion matrix between gridded product (AEMET) and the reanalysis considered (ERA5, ERA5-Land).

		Reanalysis (ERA5, ERA5-Land)	
		$P \geq 1$	$P < 1$
AEMET	$P \geq 1$	Hit (H)	Miss (M)
	$P < 1$	False Alarm (F)	CN (Correct Negative)

Mediterranean climates. On the one hand, this fact makes it highly advisable to evaluate the strengths and limitations of any reanalysis/satellite water cycle estimates before its use (Tapiador et al., 2020; Gomis-Cebolla et al., 2022). On the other hand, these rich climatic conditions make this region a perfect candidate for spatial analysis of the precipitation (Cortesi et al., 2014). In fact, Beck et al. (2019) identified that the generalizability of the findings of many studies was limited due to the consideration of small regions, which feature low spatial variability. So far, studies evaluating the performance of reanalysis precipitation products over the region, in particular ECMWF fifth generation, have been scarce. Hénin et al. (2018) evaluated ERA5 in the analysis of extreme precipitation events over the Iberian Peninsula. Tapiador et al. (2020) considered ERA5 as verification of IMERG satellite-based precipitation. In this study, with a similar approach followed in Belo-Pereira et al. (2011), Hénin et al. (2018), Beck et al. (2019), Tapiador et al. (2020), Jiang et al. (2021), Bandhauer et al. (2022) amongst others, we used a high-quality km-scale gridded precipitation product in order to evaluate ECMWF precipitation estimates. This reference precipitation dataset (Peral García et al., 2017) is provided by the Spanish Meteorological Agency and spans approximately 70 years. It has been considered as a benchmark in several hydrological applications (Senent-Aparicio et al., 2018, 2021).

In order to deeply understand the ERA5-Land/ERA5 skills we performed a comprehensive assessment which consisted in a continuous (spearman rank correlation, RBIAS, RMSE and KGE), categorical (probability of detection (POD), false alarm ratio (FAR) and HSS), pdf (histograms and Epps-Singleton test), spatial patterns (spatial pattern efficiency (SPAEF) an EOF analysis) and temporal trend (Mann's Kendall) analysis. In addition, we assessed the error dependency by precipitation intensity and orography. Depending on the analysis, multiple

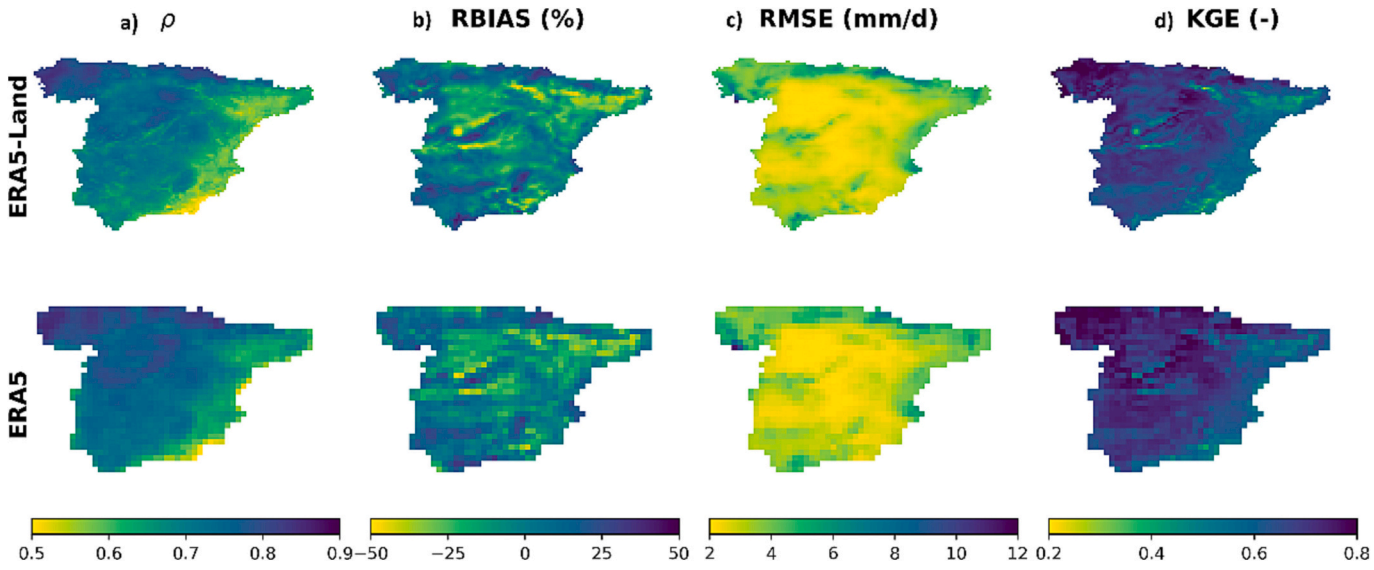

Fig. 2. Spatial distribution of ERA5-Land and ERA5 daily continuous statistics: spearman (a), RBIAS (b), RMSE (c) and KGE (d) statistics.

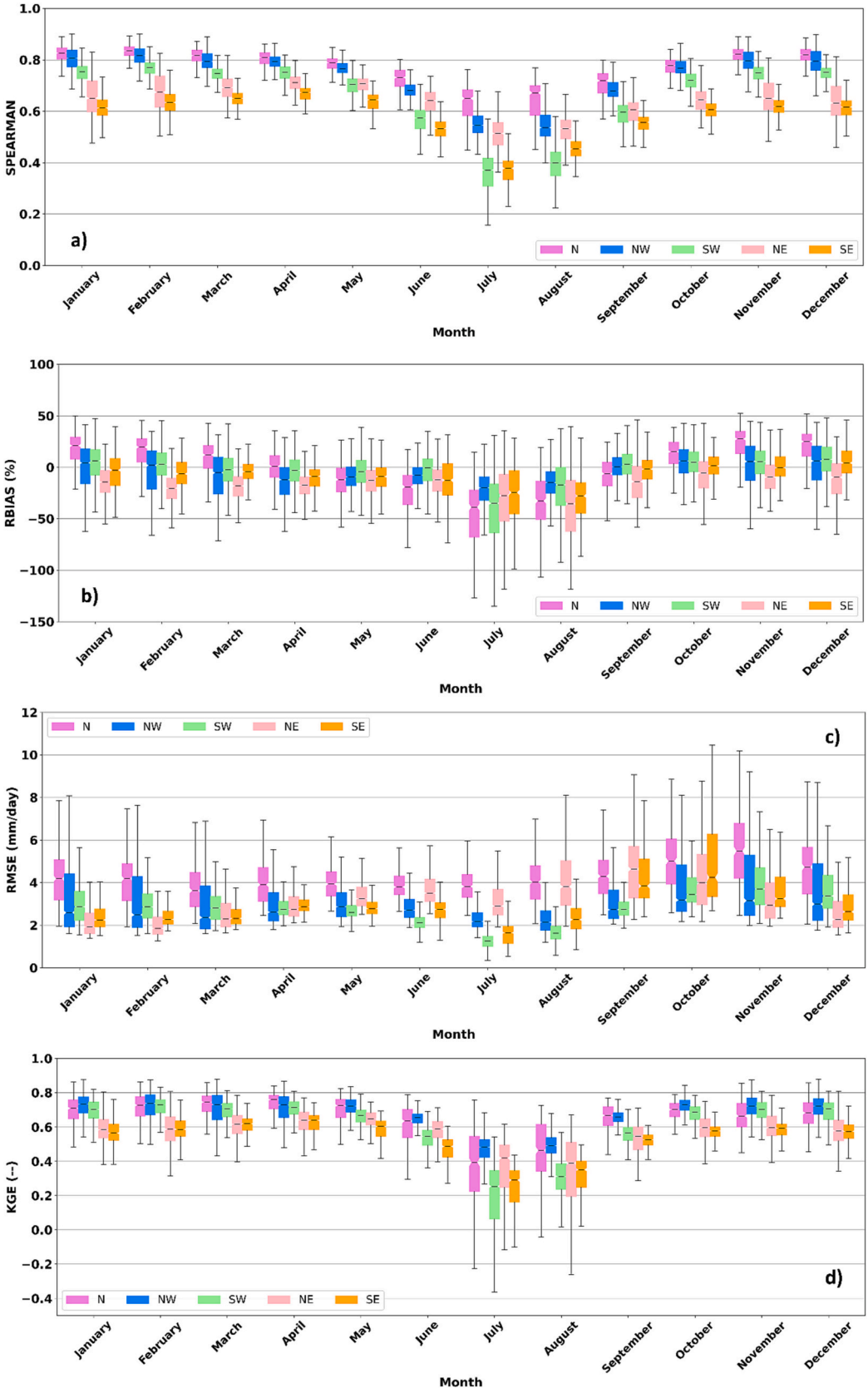

Fig. 3. Temporal evolution of ERA5-Land daily continuous statistics: spearman correlation (a), RBIAS (b), RMSE (c) and KGE (e). Outliers are not shown.

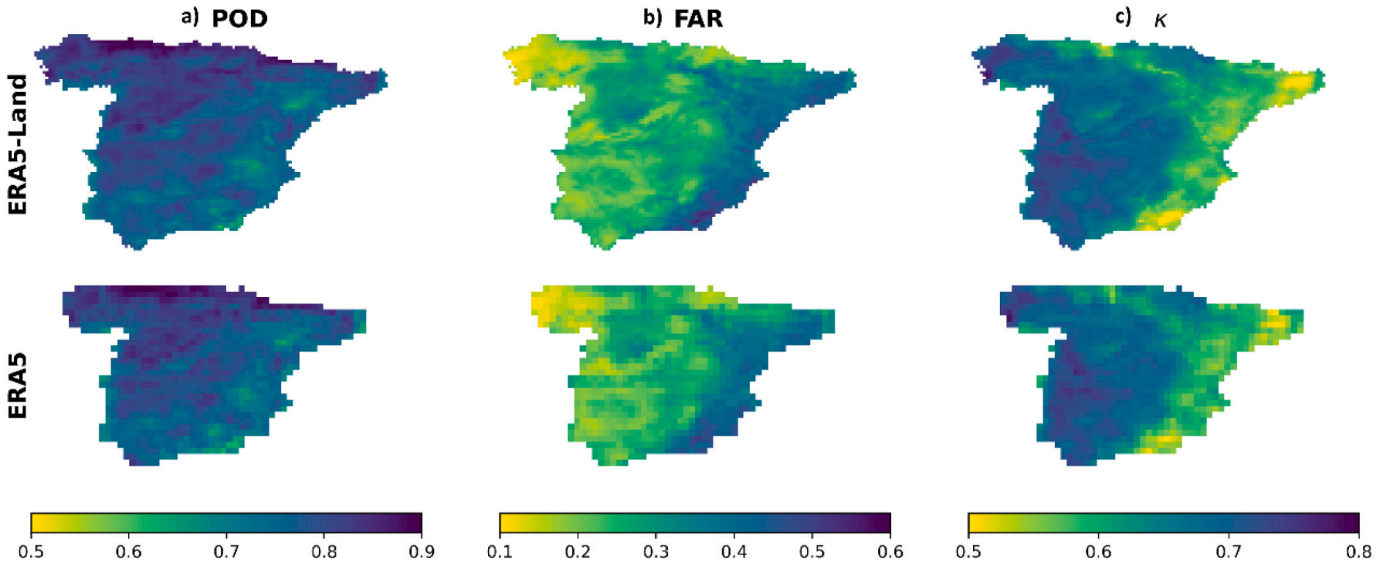

Fig. 4. Spatial distribution of ERA5-Land and ERA5 categorical statistics: POD (a), FAR (b), and Kappa (c).

temporal scales (daily, monthly and annually) have been considered.

The present paper is structured as follows. Section 2 deals with the study area's climatic/orography characterization (i.e., Spain). Section 3 summarizes the main essential features of the different reanalysis and interpolated data used. Section 4 describes the methodology employed. Section 5 summarizes the results obtained. Sections 6 and 7 deal with the discussion and conclusions of this study, respectively.

2. Study area

2.1. Study area

The study area considered is peninsular Spain [27° N - 44° N, 19° W-5° E]. The country encompasses several orographic systems (Fig. 1a): The Pyrenees (northeast), the Cantabrian mountains (across northern Spain), the Betic system (southeast), the Meseta Central, which is crossed by the Central system, the Iberian System, which extends from the eastern part of the Cantabrian Mountains to the Betic system. There are two important depressions, the Ebro River in the east and the Guadalquivir River in the southwest.

The climate of the country is highly diverse due to the orography and the spatial location between the Atlantic Ocean and the Mediterranean Sea (Serrano et al., 1999). Regarding rainfall regime, there is a sizeable latitudinal gradient in precipitation generally decreasing from north to south and from west to east, with many areas of high/low precipitation inserted in regions with opposite signs (de Castro et al., 2005). Hence, the north and north-western parts are the most humid, with mean annual precipitations records up to 2300 mm/year, while the southeast experiences 200 mm/year values (Fig. 1b). Overall, the period from October to March corresponds with more significant concentration of precipitation. Summer (June to August) is the less rainy period (Fig. 1c). The intensity of the precipitation is higher on the coast, especially on the Mediterranean coast according to the Climate Atlas of Spain (see http://atlasnacional.ign.es/wane/Clima).

3. Datasets

3.1. Observed precipitation datasets

The Spanish Meteorological Agency, with the objective of climate monitoring, provides a high resolution gridded (5 km × 5 km in rotated grid) daily precipitation product spanning the 1951–2020 period. Precipitation estimates were produced using the optimal interpolation method and considering the Surface Parameters Analysis (SPAN) system (Rodríguez et al., 2003; Navascués et al., 2003; Quintana-Seguí et al., 2016) which was appropriately adjusted to represent the structures of 24 h precipitation at the scale allowed by the density of stations (Peral García et al., 2017). A total of approximately 3236 gauges stations across peninsular Spain and Balearic Islands were considered in the analysis. Precipitation estimates represent the precipitation accumulated between 07 UTC of day n and 07 UTC of day n + 1 (Peral García et al., 2017). Details of the products are summarised in Table 1. This dataset is used as a benchmark to evaluate the ERA5 and ERA5-Land performance.

3.2. ERA5 reanalysis precipitation datasets

ERA5 is the fifth generation of the ECMWF reanalysis. It is based on the Integrated Forecasting System (IFS) Cy41r2. Measurements from different observations systems (satellite, in-situ data, etc.) are integrated into the atmospheric model using a 4D-Var scheme (Hersbach et al., 2020). It also provides a physically consistent analysis of the land surface and ocean by coupling the atmospheric part of the IFS with the land-surface model HTESSEL and the ocean wave model (WAM). ERA5 resolves the atmosphere using 137 hybrid sigma/pressure (model) levels from the surface up to 1 Pa. The grid resolution is 31 km (0.218125°). Data are available hourly and consist of analysis and short forecasts, which run twice daily from 06 and 18 UTC. Uncertainty estimates for all variables are also provided at a reduced spatial and temporal resolution. ERA5 provides global spatial coverage from 1950 until the present.

ERA5-Land is a spatially enhanced version (9 km). It results from forcing the HTESSEL land surface component (version Cy45r1 of the IFS) with low atmospheric meteorological fields from ERA5. Observations only influence the simulation indirectly through the forcing, no atmospheric/oceanic coupling or data assimilation scheme is considered (Muñoz-Sabater et al., 2021) This is achieved in order to dispose of a computational affordable updateable version. Data are provided from 1950 to the present at an hourly resolution over land regions (i.e., all oceans are masked).

Both reanalyses are available from the Copernicus Climate data store. These products come interpolated at a regular latitude/longitude grid (netcdf format) of 0.25° x 0.25° and 0.1° x 0.1° for the case of ERA5 and ERA5-Land, respectively. In this study, we downloaded hourly forecast precipitation data (total precipitation) for the study period (1951–2020) over peninsular Spain. Details of the products are summarised in Table 1.

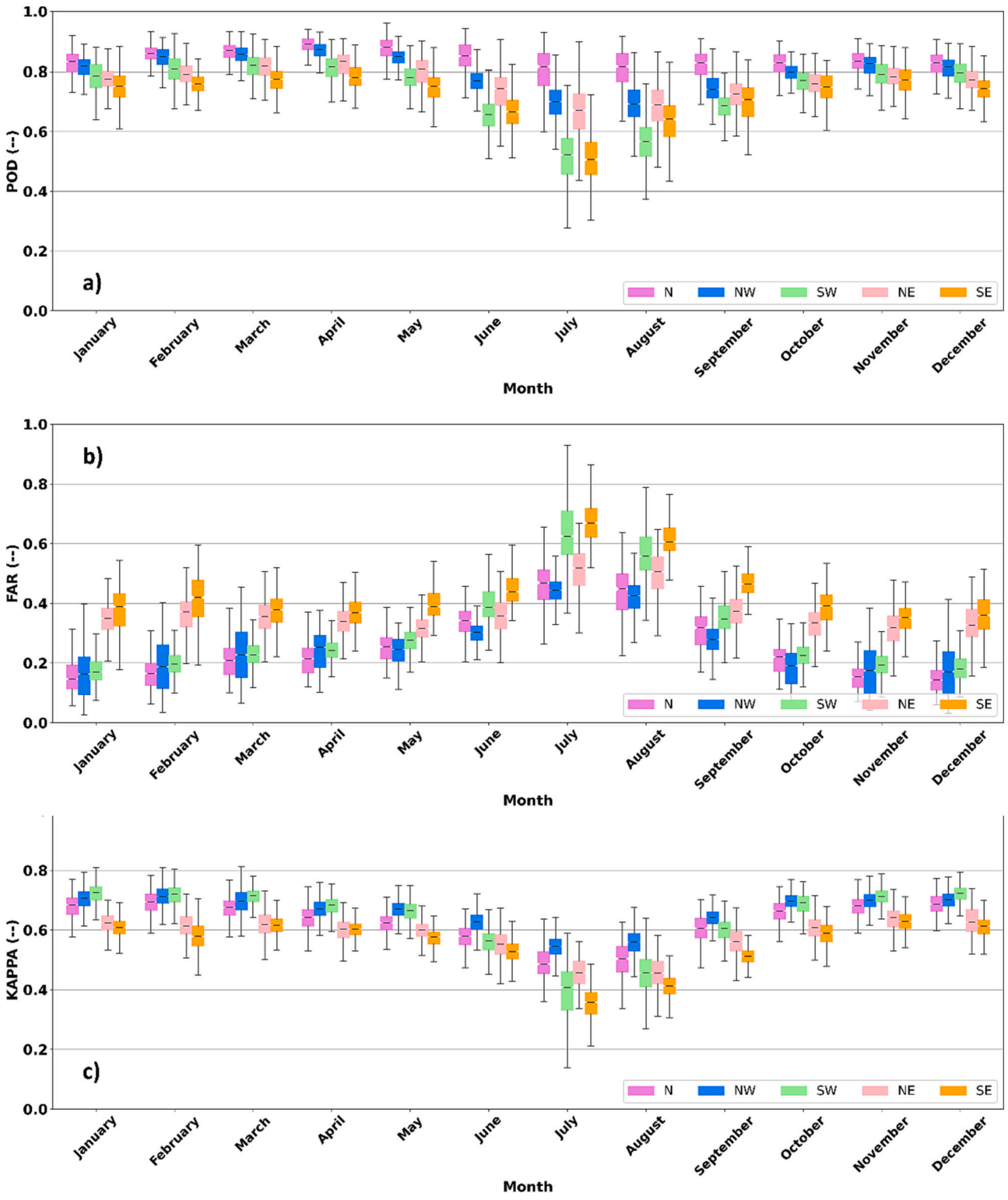

Fig. 5. Temporal evolution of ERA5-Land categorical statistics: POD (a), FAR (b), Kappa (c).Outliers are not shown.

4. Methods

4.1. Pre-processing of the datasets

ERA5 and ERA5-Land datasets, available at hourly timesteps, were aggregated to obtain daily time step values matching the observed gridded products time observations (07 h UTC to 07 h UTC). In addition, to enable a consistent comparison, AEMET dataset was resampled to 0.1° (0.25°) grid-cell size for ERA5-Land (ERA5) respectively. Prior to this step, AEMET rotated grid was resampled to a regular 0.05° grid using nearest neighbour interpolation.

4.2. Continuous assessment

Table 2 summarizes the statistics considered in the continuous analysis. The spearman rank correlation (ρ) provides an assessment of

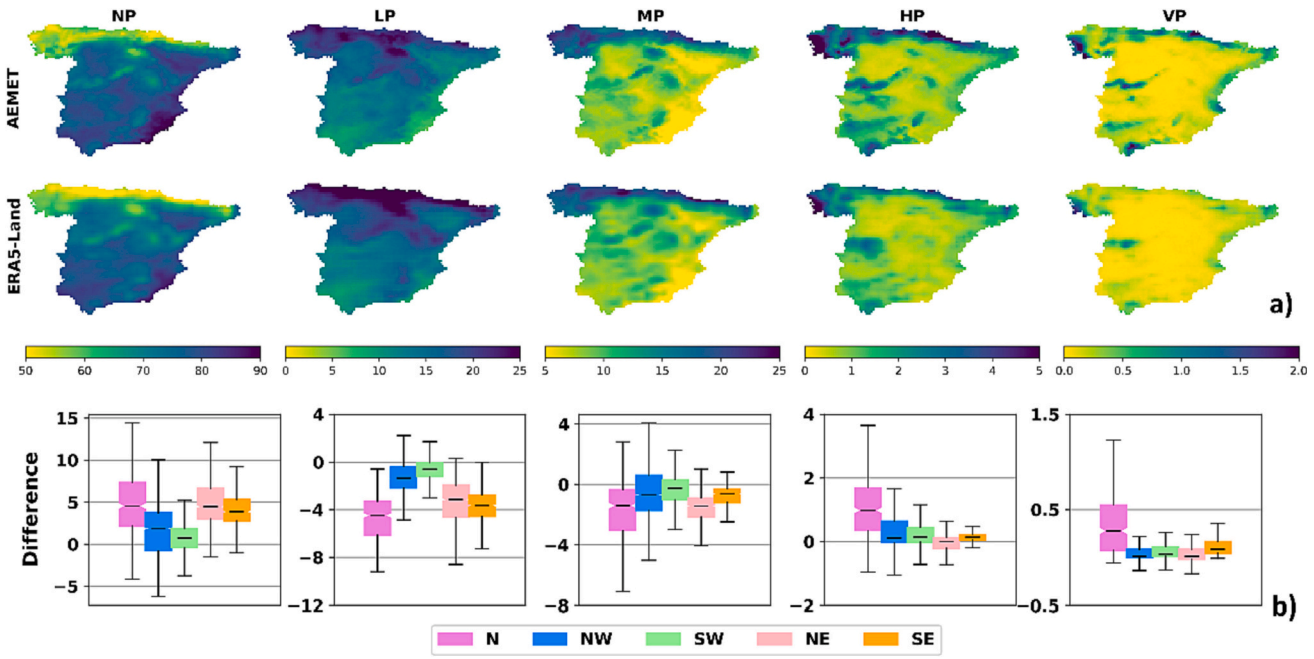

Fig. 6. Spatial distribution of AEMET and ERA5-Land histograms (a) and boxplots of the differences (b).Outliers are not shown.

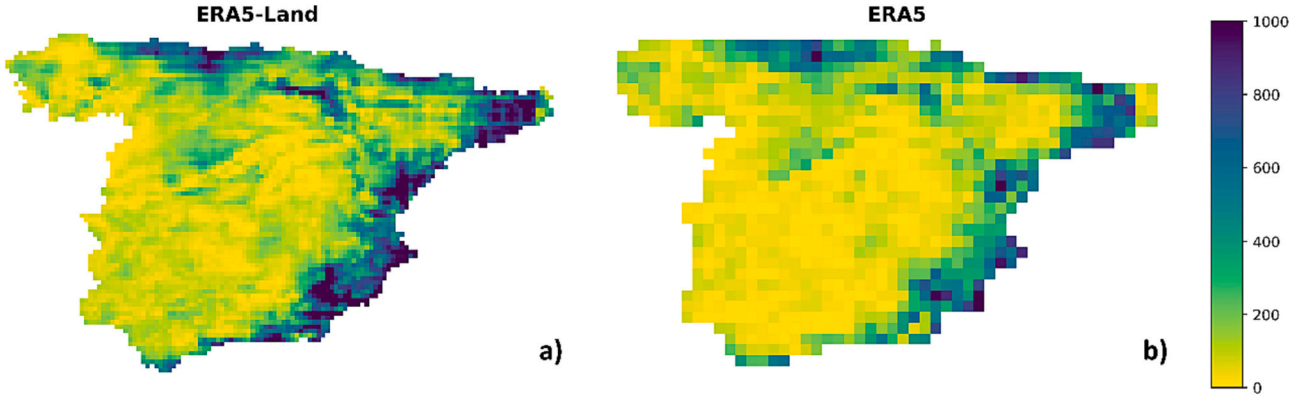

Fig. 7. Eps-Singleton statistics for ERA5Land (a) and ERA5 (b). The higher the value the higher the discrepancy amongst the pdfs of the datasets.

how well the relationships between two variables can be described using a monotonic function. Contrary to commonly applied correlation coefficient, this non-parametric statistic does not require data to be normally distributed. RBIAS describes the systematic bias of precipitation estimates, underestimation (RBIAS>0%) or overestimation (RBIAS<0%). RMSE is able to quantitatively represent the error characteristics between reanalysis estimates and observed data. KGE provides a measure of model performance considering the mean, the variability and the temporal dynamics. The non-parametric version described in Pool et al. (2018) was considered in this study. These statistics were calculated at daily, monthly and yearly timesteps for the period 1951–2020 using hydroeval package (Hallouin, 2021). Temporal evolution of these statistics was calculated over climatic regions which were defined by applying a k-means clustering to AEMET monthly precipitation anomaly time series. In order to set the appropriate number of clusters we used the heuristic elbow method (i.e. plotting the explained variation as a function of the number of clusters and check for the elbow of the curve) (Manzano et al., 2019) (Fig. S1). The resulting precipitation regions agree with those proposed in previous works (Belo-Pereira et al., 2011; Manzano et al., 2019).

4.3. Categorical assessment

Precipitation event detection was assessed considering the statistics listed in Table 2. The Probability Of Detection (POD) and False Alarm Ratio (FAR) represents the ratio of correctly or falsely detected precipitation occurrences by the reanalysis to the total number of detected precipitation occurrences. Heidke skill score (HSS), known also as Cohen's Kappa, measures the classification accuracy relative to that expected by chance. Categorical indices were derived considering the confusion matrix in Table 3. Chi Square test of independence was additionally used in order to check the statistical relationship between the datasets. Categorical assessment was obtained for the 1951–2020 period considering data at daily timesteps only. Event threshold was set to 1 mm/day (Chen et al., 2020; Xin et al., 2021). Same climatic regions as Section 4.2 were considered for temporal evolution assessment.

4.4. PDF assessment

The capability of the reanalysis estimates to reproduce the frequency distribution of the observed data was obtained by comparing the histograms of both datasets under different precipitation intensity levels. Daily based events were discretized into five threshold (Acharya et al.,

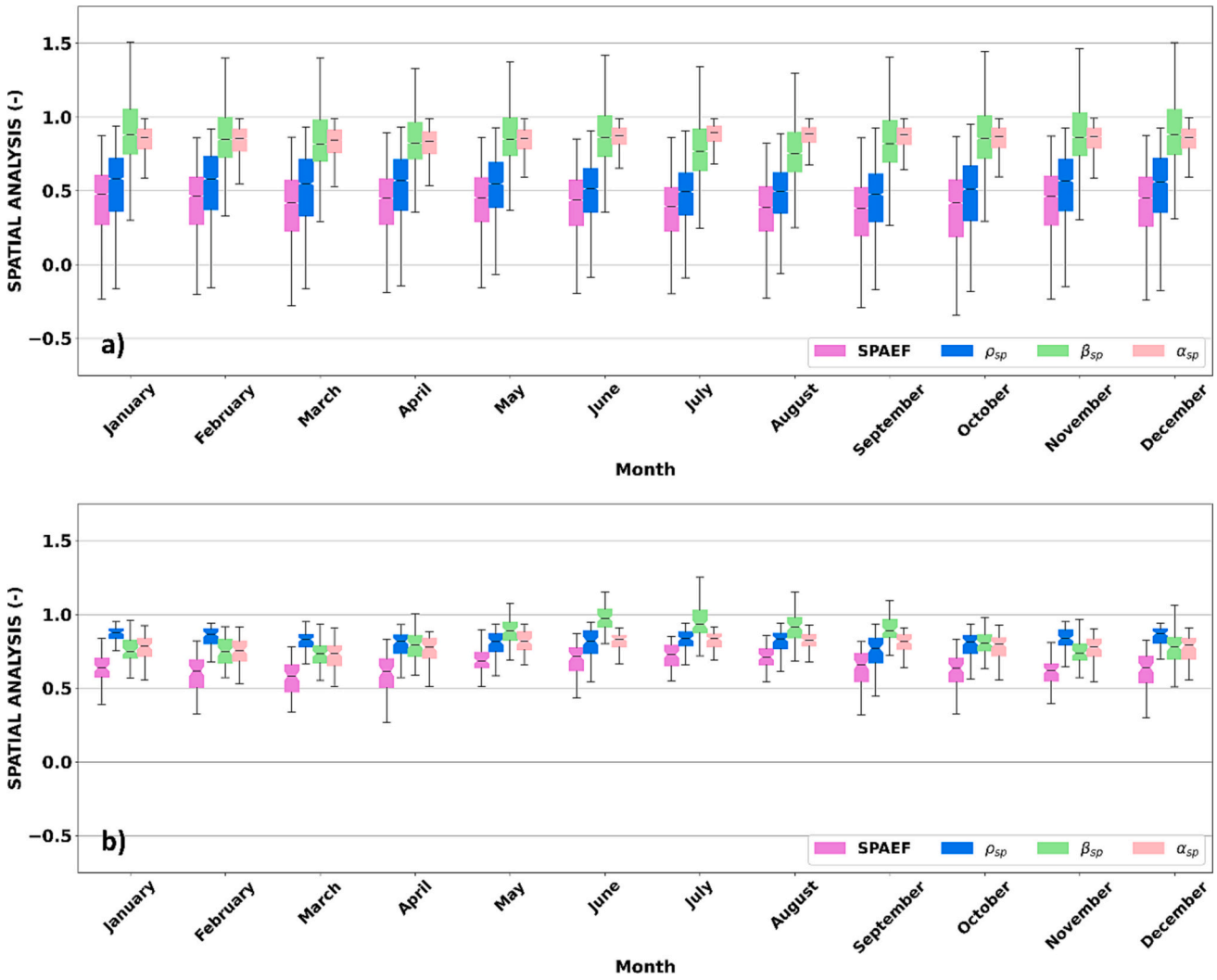

Fig. 8. ERA5-Land SPAEF daily (a) and monthly (b) values. Outliers are not shown.

2019; Amjad et al., 2020). They are: no precipitation (NP) (< 1 mm/day), light precipitation (LP) (≥1 and < 5 mm/day), moderate precipitation (MP) (≥5 and < 20 mm/day), heavy precipitation (HP) (≥20 and < 40 mm/day) and violent precipitation (VP) (≥40 mm/day). In addition to this, we also applied the Epps-Singleton test. It is based on the empirical characteristic function and has shown a higher power than the traditional Kolmogorov-Smirnov test in many applications (Epps and Singleton, 1986). Under the null hypothesis the test demonstrate that observed and reanalysis estimates come from the same continuous distribution.

4.5. Spatial pattern evaluation

The capability of the reanalysis in order to reproduce the precipitation spatial distribution (i.e., spatial patterns) was assessed using SPAEF statistic (Table 2) and EOF analysis. SPAEF considers three equally weighted components: spatial correlation coefficient (ρ_{SP}), the fraction of the coefficient of variation (β_{SP}) which provides a representation of the spatial variability and histogram overlap (α_{SP}) which helps to emphasize non-existing spatial variability between regions of high and low values (Koch et al., 2018). α_{SP} is computed considering z-scores in order to ensure bias insensitivity. We replaced the correlation coefficient by spearman rank correlation in order to consider the non-normality of the precipitation. SPAEF statistic was calculated over the region of study at daily/monthly/yearly timesteps.

Empirical Orthogonal Function (EOF) analysis is able to decompose a spatio-temporal dataset into a set of orthogonal spatial patterns (EOFs) along with a time series of coefficients (principal components, PCs) that control their time variation. In addition, they do also provide a measure of the importance of each pattern (variance explained). In this way the dimensionality of the dataset is reduced to a small number of representative components. EOF analysis was applied in T-mode in order to focus on the identification of spatial patterns. Analysis was performed considering monthly and daily timesteps. The time and space average of the precipitation data has been subtracted from the product considered before the EOF analysis.

4.6. Temporal trends

Similarities and differences in the temporal trends of the datasets were assessed considering non-parametric Mann's Kendall test and Sen's slope estimator. In Mann's Kendall test, the null hypothesis (H0) indicates no-trend presence, while the alternate hypothesis (H1) indicates monotonic trend (increasing or decreasing). While no assumption about the data distribution is needed, the test requires the data to be serially independent. In order to reduce the impact of autocorrelation two approaches have been suggested in the literature: variance correction (explicit calculation of the inflated variance) and prewhitening method (removing the lag-1 autoregressive process). In this study, Hamed (2009) and Yue and Wang (2002) methods, being representative of both

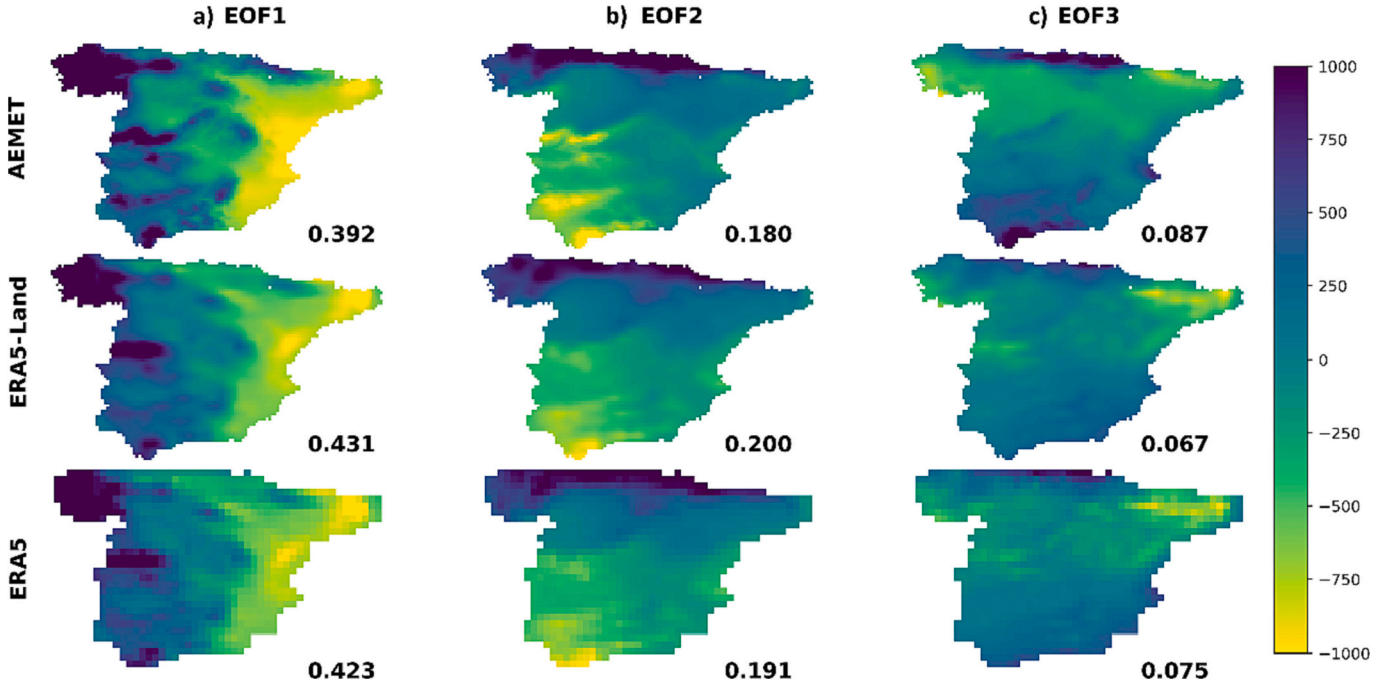

Fig. 9. First (a), second (b) and third (c) EOFs for ERA5-Land and ERA5 considering monthly time series. Associated number refers to the variance explained.

approaches, were also applied as an independent verification of the effect of serial autocorrelation. Both provide a modified Sen's slope. They are available from the Modifiedmk R package (Patakamuri and O'Brien, 2021), Trend analysis was applied independently to AEMET and ERA reanalysis precipitation time series considering seasonal and yearly total amounts. Seasons were defined as: winter (DJF), spring (MAM), summer (JJA) and autumn (SON).

4.7. Error dependency with precipitation intensity and orography

The influence of precipitation intensity on model performance was assessed by analysing continuous (ρ, RBIAS, RMSE and KGE) and categorical metrics (POD and FAR) across the previous precipitation categories (Section 4.3). In this case, hits represent the matches between AEMET and ERA5-Land/ERA5 for a specific category, while false alarm or misses represent the totality of the non-matches across the different categories (see Table S1 in supplementary material). Precipitation categories were defined from observational AEMET. Assessment was performed considering daily timestep values over the 1951–2020 period. Influence of orography was assessed by calculating the spatial spearman correlation between the RBIAS/RMSE/KGE/κ metrics and elevation (m) / slope (%). Results were provided at country and climatic region level. Boxplots were considered for visual representation of the relationships. Elevation was obtained from Spanish Geographic Institute at 200 m. QGIS v3.26.1 ('Buenos Aires') was used to calculate the slope. Both raster images were resampled using spatial averaging to 0.1° (ERA5-Land) and 0.25° (ERA5) spatial resolution.

5. Results

5.1. Continuous assessment

Spearman correlation (Fig. 2a) and KGE (Fig. 2d) show a spatial gradient from north-west (highest values) to south-east (lowest values). KGE however provides a more complex spatial pattern with poor KGE performance in inner locations of the country apart from the eastern coast. The coexistence of regions of opposite sign in small regions (the Pyrenees and the Central System) difficult the regional characterization of RBIAS (Fig. 2b). Nevertheless, predominant areas of underestimation/overestimation are located in the N/NE. RMSE (Fig. 2c) lowest values (2 mm/d to 4 mm/d) are spatially distributed mostly in the centre of the country. Highest values (up to 12 mm/d) are distributed also across the borders of the country with special emphasis over the N region. Monthly and yearly analysis (Fig. S2 and S3) generally reproduce the same spatial patterns of the daily assessment.

Worst model performance is observed during the June–September months as shown by the decrease in KGE (Fig. 3d) and spearman correlation (Fig. 3a) (KGE/spearman median values ranging approximately from 0.2/0.4 to 0.5/0.7). The spatial gradient in Fig. 2 persists for these two statistics during all the year. Nevertheless, SW ranks worse or similar to SE for the July–August months. General overestimation is also observed during these months and along all the year for NE region (Fig. 3b). Largest underestimation is provided by N region during November – February months. Overall, RMSE (Fig. 3c) peak at the end of the year (N-NW-SW in November, NE in September and SE in October). Monthly RMSE variability is also greater for this period and during winter months (January–April) for N and NW. Conclusions derived from this analysis still hold true when considering monthly analysis (Fig. S4). ERA5 analysis results are analogous (Fig. S5 and S6).

5.2. Categorical assessment

A fair agreement is observed between the two datasets ($0.4 < \kappa < 0.8$) (Fig. 4c). Nevertheless, north and centre of the country (N, NW and SW) generally provide a better detection capability (Fig. 4a) and a lower number of false alarm events (Fig. 4b) than the eastern coast (NE and SE). Significant statistical relationship is confirmed by the Chi Square (Fig. S7) test of independence (all pixels having values of p-value < 0.05). Chi square statistic provides a similar spatial distribution to Kappa statistic. Both statistics indicate a substantial agreement ($0.6 < \kappa < 0.8$) for NW and SW while a moderate agreement ($0.4 < \kappa < 0.6$) for SE and NE (Fig. 4c).

Same conclusions as in the continuous assessment are obtained for the temporal evolution of statistics: worse performance (i.e., lower POD (Fig. 5a) and Kappa (Fig. 5c) and higher FAR (Fig. 5c)) obtained during summer months (June–September) and similar spatial gradient which

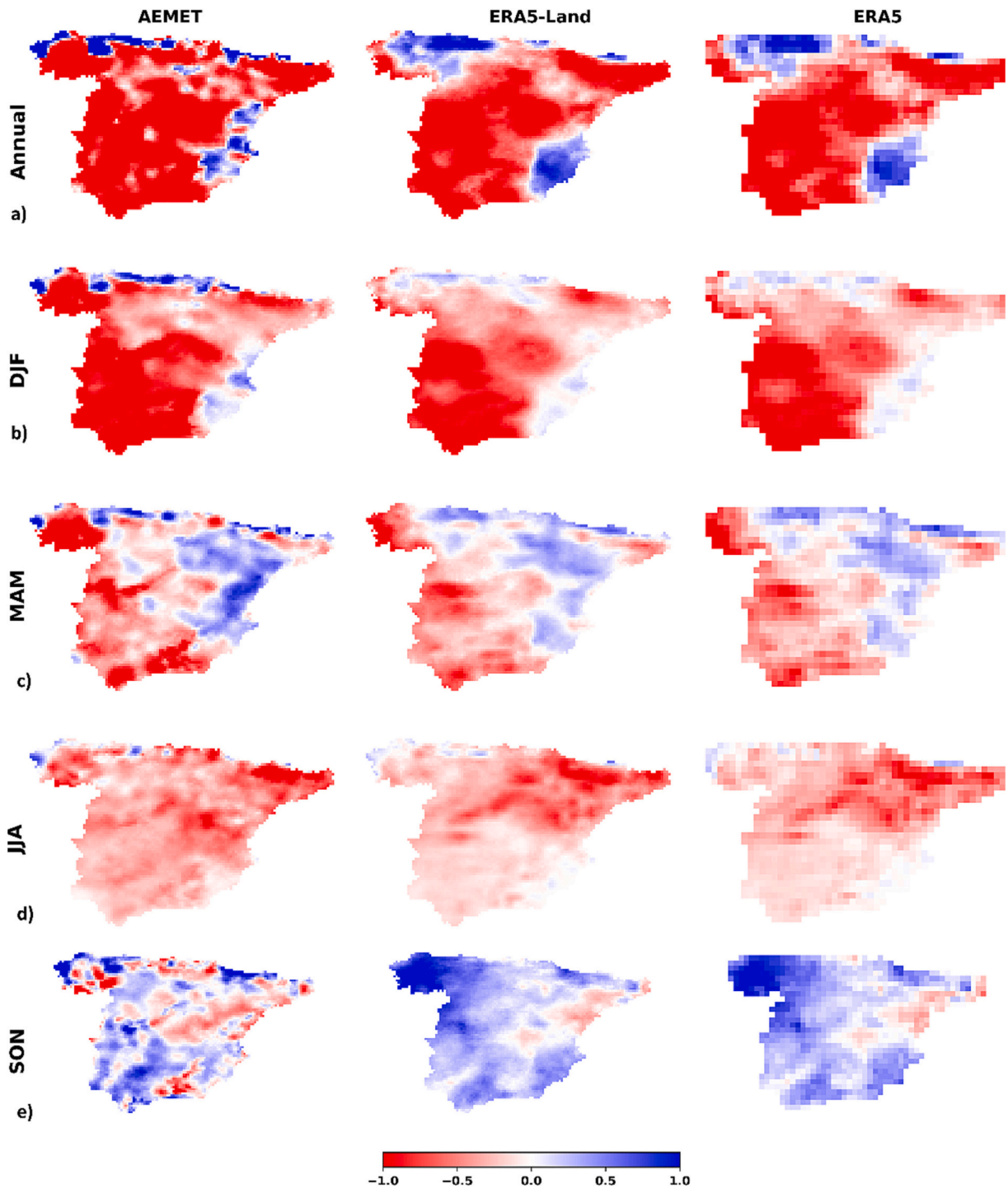

Fig. 10. AEMET, ERA-Land and ERA5 annual (a) and seasonal (b-e) Sen's slope (mm/y).

persists along the year. Analogous conclusions are obtained for ERA5 categorical analysis (Fig. S8).

5.3. PDF assessment

Overall, it is observed ERA5-Land generally reproduces the frequency distribution of AEMET dataset in terms of spatial location (Fig. 6a) but not in terms of magnitude (Fig. 6b). Generally, ERA5-Land tends to underestimate the NP/HP/VP categories, while overestimating the LP/MP. NP provides the greatest deviation. For the different regions, NW and SW tend to provide a better performance (i.e., less underestimation/overestimation) than the N, NE and SE (Fig. 6b). N provides the greatest deviation for the HP and VP categories. N and SE show signs of underestimation (Fig. 6b). ERA5 pdf assessment is displayed in Fig. S9. Analogous conclusions are obtained.

Fig. 7 displays the result of the ERA5-Land and ERA5 Epps-Singleton statistic test. No statistically significant (at 95%) agreement between pdf is obtained. The eastern coast of Spain together with part of the northern region provides the major discrepancy amongst the AEMET and ERA5-Land probability distribution functions thus confirming previous findings from Fig. 6.

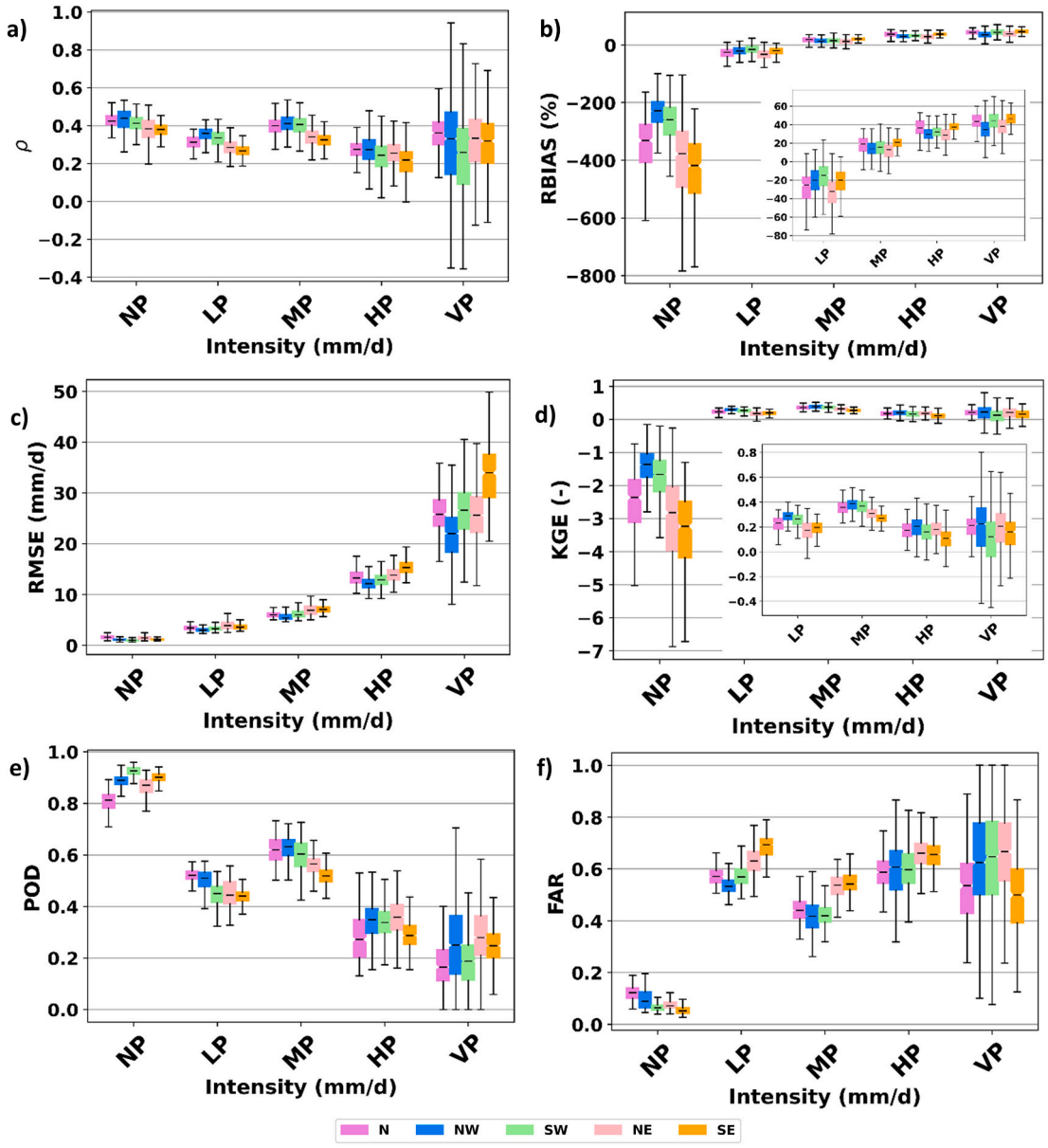

Fig. 11. Spearman (a), RBIAS (b), RMSE (c), KGE (d), POD (e) and FAR (f) by precipitation categories for ERA5-Land. Outliers are not shown.

5.4. Spatial pattern evaluation

ERA5-Land properly reproduces the spatial patterns provided by AEMET at both daily (Fig. 8a) and monthly (Fig. 8b) timesteps (SPAEF>0.5). All the three components confirm the good performance. Greater variability and lower SPAEF values are observed at daily scale. Seasonal dynamics is not as pronounced as in the continuous and categorical assessment. A proper reproduction of the spatial patterns (SPAEF values in the range [0.60–0.90]) is also obtained at the yearly timescale. ERA5 analysis (Fig. S10) provides analogous findings.

Fig. 9 displays the EOFs for both AEMET and ERA5-Land/ERA5 at monthly scale (daily scale results in Fig. S11). The resulting spatio-temporal decomposition of AEMET and ERA5-Land/ERA5 is similar. Main discrepancies arise at the third EOF (Fig. 9c). AEMET EOF is spatially more enhanced than ERA5 and ERA5-Land, with a special emphasis over the northern, southern and part of the eastern coast.

5.5. Temporal trends

ERA5-Land and ERA5 properly reproduce the most important spatial features of AEMET trend at annual scale (Fig. 10a). The three datasets reproduce a decrease for the whole country in exception of the north-west and south-east (and in a minor extent the Pyrenaic region) which experiment positive trends. It is worth noting that differences exist in the exact location, spatial extent and magnitude of these positive trend regions. At seasonal scale, SON season shows the most discrepant behaviour between the datasets, with ERA5-Land and ERA5 not properly reproducing the regions with negative trend. For the rest of the seasons, a similar spatial reproduction is observed with changes in absolute values of the trend. Comparison with the independent verification (Fig. S12 and Fig. S13) did not reveal any remarkable difference in the spatial distribution of the trend values. Statistically significant trends (p-value <0.05) where obtained mostly for AEMET dataset (Fig. S14–16).

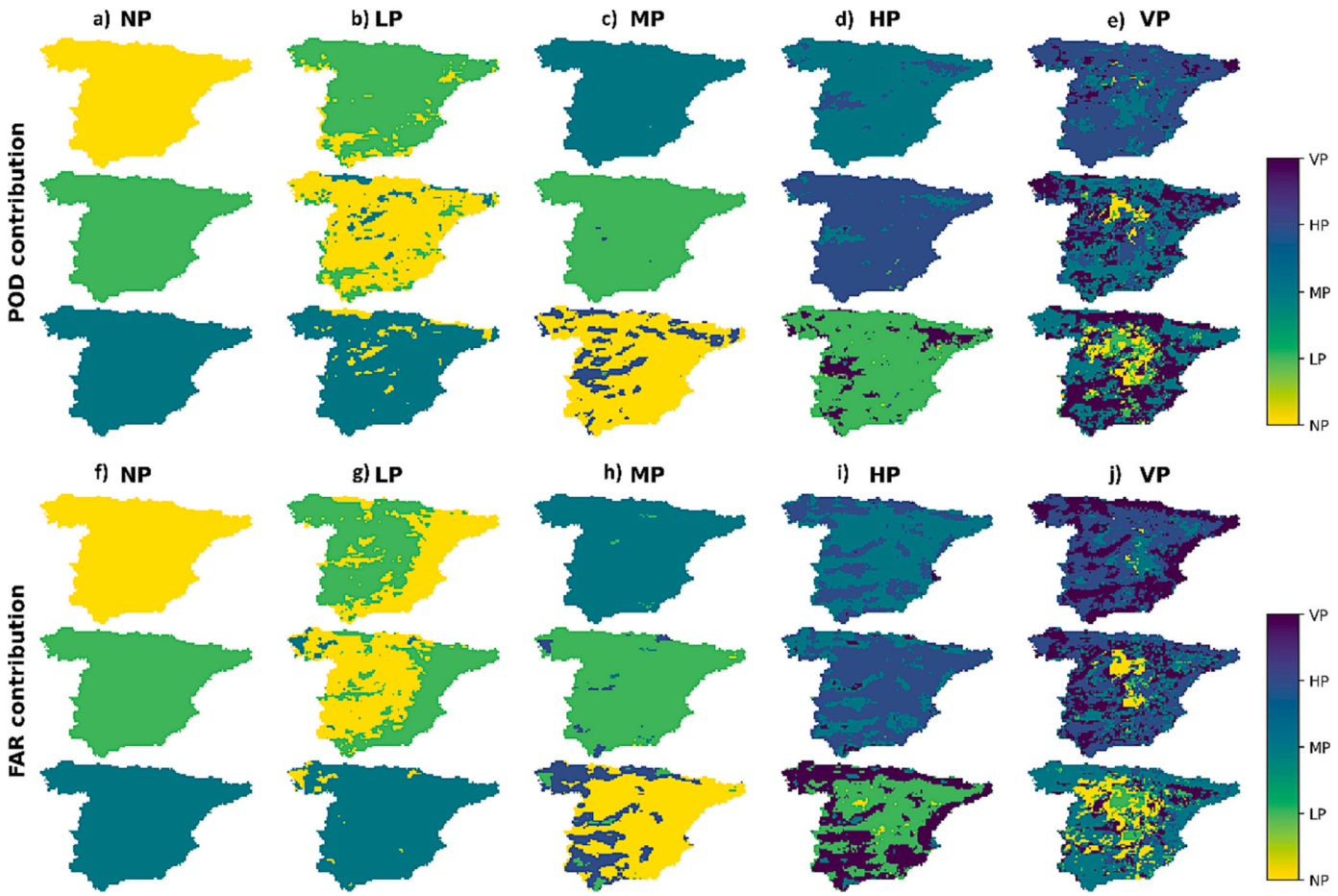

Fig. 12. POD (a-e) and FAR (f-j) contribution for ERA5-Land. Only the first, second and third categories with a higher number of misses and false alarms are displayed (i.e., in Table S1 for each row we select for an AEMET category the corresponding ERA5-Land categories with a higher number of events and the same but column-wise). A category ideally classified would be itself for the 1st, 2nd and 3rd category (i.e., misses and false alarms having null values).

5.6. Error dependency with precipitation intensity and orography

Error analysis revealed continuous and categorical statistics are intensity-category and region dependent. Spearman correlation (Fig. 11a) shows a higher variability for the HP and VP categories. Same spatial gradient as in Section 5.1 is observed. NP and MP generally provide the best correlation (i.e., higher median value and less variability). RBIAS (Fig. 11b) displays overestimation for NP and LP while underestimation for MP, HP and VP. Underestimation increases as it does the precipitation intensity. Generally, NW and SW provide the best RBIAS performance (i.e., closer to null values). RMSE (Fig. 11c) increases with precipitation category. Eastern regions provide the highest RMSE values, especially SE in VP. KGE (Fig. 11.d) shows greater variability for NP and VP. MP provides the best KGE performance. POD (FAR) (Fig. 11e-f) decreases (increases) with precipitation category. There is a good no-precipitation detection capacity, as indicated by the high and low POD and FAR values, respectively. N region ranks the worst while eastern regions provides an acceptable performance. Other categories provide an opposite spatial behaviour (i.e., eastern regions ranking worst), especially for LP and MP categories. A jump in performance is observed for MP category (i.e., better performance than LP). VP and HP show a higher spatial variability than the other categories. Same conclusions could be derived for ERA5 (Fig. S16).

Fig. 12 assesses misclassifications between categories. Same conclusions could be deduced for ERA5 (Fig. S17). Generally, misclassifications tend to occur between neighbour categories (i.e., NP is wrongly assigned to LP or MP but not VP). NP category is well classified. Most of AEMET events are classified as NP by ERA5-Land, and the misses are assigned to the LP and MP categories respectively (Fig. 12a). False detections additionally follow this order (Fig. 12f). For LP category, ERA5-Land detects the most part of AEMET LP events (Fig. 12b). Nevertheless, over the Mediterranean coast it falsely classifies as LP AEMET NP events (Fig. 12g). Misclassifications in the MP category are assigned to LP category followed by the NP and HP categories (Fig. 12c). Spatial heterogeneity in the misclassifications increase for HP and VP (Fig. 12 d-e). In addition, HP and VP categories are not well represented (i.e., the number of misses and false alarms are higher than the HP and VP detected events). HP misclassifications are attributed to the MP category (Fig. 12d). LP representing the third contribution to ERA5-Land misses (Fig. 12d). Focusing over areas of extreme events occurrence (Fig. 6a, AEMET VP), ERA5-Land does not tend to falsely detect the VP events (Fig. 12j) nevertheless, an important part of these is missed (Fig. 12e) (i.e., it properly classified a small part of the events).

KGE model performance (Fig. 13g-h) remains constant as a function of orography. Weak spatial correlation in Table 4 supports this fact. Nevertheless RBIAS (Fig. 13a-b), RMSE (Fig. 13c-d) reveal to be more dependent on elevation and slope. Both statistics show an inflexion point at 1000 m (Fig. 13a,c). Spatial correlation (Table 4) does not indicate a strong relationship between these two variables and the elevation. Slope behaviour is different. RBIAS shows signs of underestimation (overestimation) for slope values >20% (< 10%). 10–20% category provides the less deviated performance. RMSE shows an increase with slope. Spatial correlation (Table 4) reveals a strong relationship with slope, especially for RMSE. Kappa score (Fig. 13e-f) shows a slight decrease with elevation and slope, which is supported by the weak correlation in Table 4. Similar conclusions are derived for ERA5 (Fig. S18 and

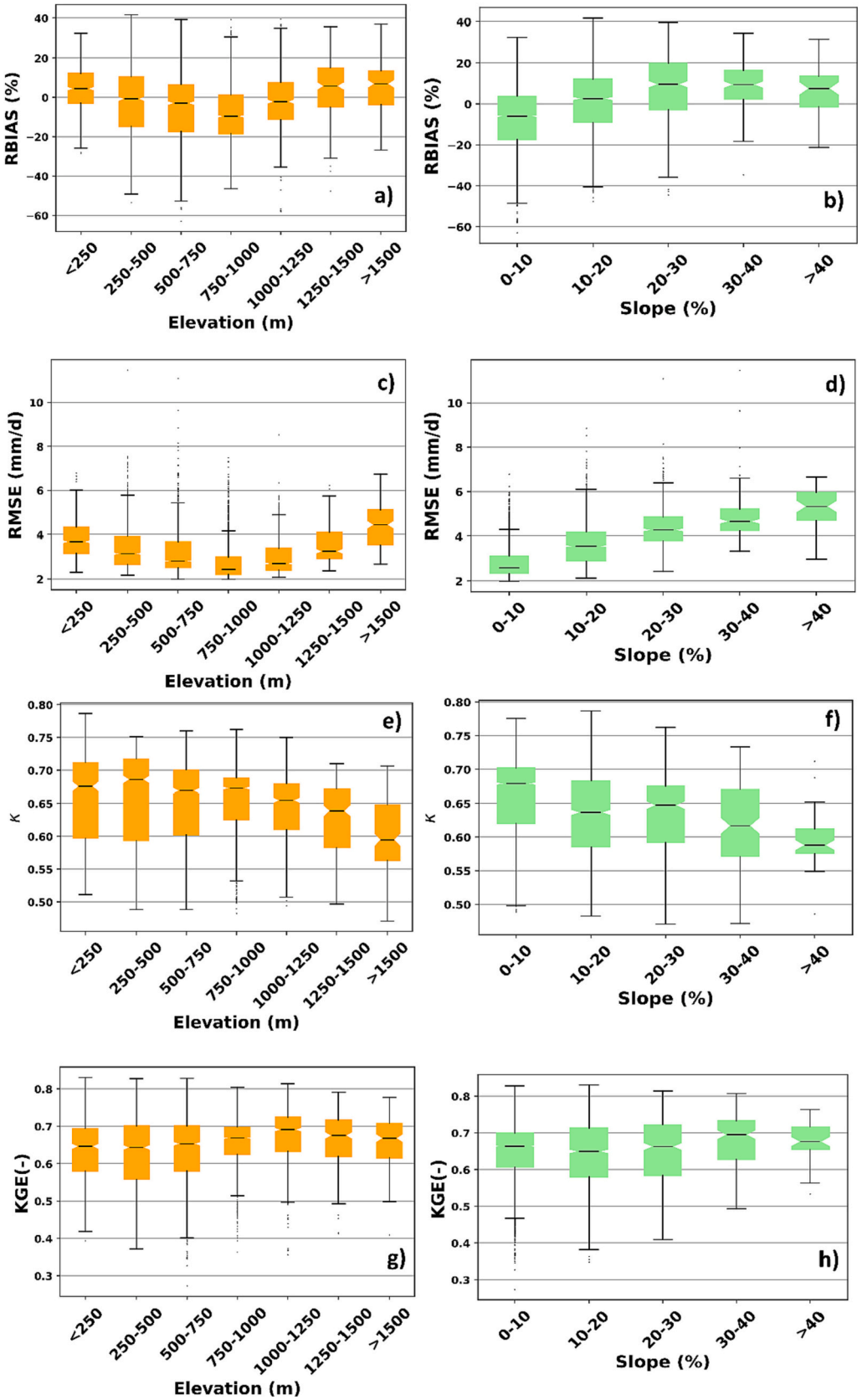

Fig. 13. RBIAS (a-b), RMSE (c-d), Kappa (e-f) and KGE (g-h) dependency with elevation and slope for ERA5-Land.

Table 4
Spatial spearman correlation of RBIAS, RMSE, Kappa and KGE with elevation and slope for the climatic regions and whole country (ERA5-Land). Significant correlation (p-value <0.05) is indicated by *.

	Elevation (m)				Slope (%)			
	RBIAS	RMSE	Kappa	KGE	RBIAS	RMSE	Kappa	KGE
N	0.024	−0.200*	−0.060	−0.110*	0.340*	0.650*	0.130	0.270*
NW	0.006	−0.110*	−0.500*	−0.270*	0.710*	0.830*	0.010	0.370*
SW	−0.159*	−0.240*	−0.550*	0.050*	0.480*	0.510*	−0.240*	−0.110*
NE	0.345*	0.050	0.140*	0.580*	0.340*	0.640*	−0.240*	0.240*
SE	−0.269*	−0.280*	−0.210*	0.320*	0.004*	0.390*	−0.290*	−0.180*
Spain	0.064*	0.198*	−0.197*	0.150*	0.412*	0.690*	−0.290*	0.060*

Table S2).

6. Discussion

6.1. Model performance

6.1.1. Continuous-categorical-pdf assessment

Continuous assessment of precipitation revealed a general good agreement between AEMET observations and ERA5-Land/ERA5 estimates, documented by KGE values > 0.4 (behavioural), high correlation values (0.5–0.9) and low values of RMSE (mostly between 2 and 8 mm/d) (Fig. 2). Categorical assessment also indicated a good agreement (kappa values between 0.4 and 0.8) (Fig. 3). Both assessments however revealed a dependence of the performance with the spatial location. Correlation displayed a NW-SE spatial gradient, which share some similarities with KGE and kappa spatial distribution, especially over the Mediterranean coast and the Ebro River basin. Similar spatial behaviour was reported by Belo-Pereira et al. (2011) over the Iberian Peninsula (IP) when considering ERA-40 and ERA-Interim (i.e., ERA5/ERA5-Land predecessor). This behaviour can be related to the climatic characteristics of the study area: while in the N, NW and SW regions precipitation depends particularly on synoptic-scale disturbances, in the NE and SE precipitation shows a more complex variability (Cortesi et al., 2014). Over semiarid areas, such as the eastern coast, precipitation is often a local phenomenon (Tapiador et al., 2020). Especially, over these regions (NE and SE) deteriorated POD and FAR statistics (Fig. 3) indicated that ERA5-Land/ERA5 reanalysis were misclassifying AEMET dry days (i.e., no precipitation) as wet days (i.e., precipitation >1 mm). This wet bias (dry days poor detection capacity) has been also documented in IP by Hénin et al. (2018) and in other world regions (el Kenawy et al., 2015; Beck et al., 2017; Amjad et al. (2020)). RBIAS (Fig. 2c) displayed signs of overestimation and underestimation. Overestimation has been commonly reported for ERA5 (Crossett et al., 2020; Amjad et al., 2020; Bandhauer et al., 2022). Nevertheless, underestimation has been also indicated by Kolluru et al. (2020) and by Longo-Minnolo et al. (2022). A clearly uniform RBIAS behaviour is difficult to observe for regions of high climatic complexity (Beck et al., 2019; Sharifi et al., 2019; Jiang et al., 2021). RMSE high values spatially distributed across the northern and eastern coast might be partially attributed to the closeness to the sea due to the more-complex breeze circulation and coastal convection systems (Caracciolo et al., 2018; Lockhoff et al., 2019). Nevertheless, AEMET associated uncertainty due to station density is also a factor to consider, especially over the northern regions such as Galicia.

Worst performance was observed in summer months for both the continuous and categorical assessment. The shift in the median together with the wider boxes and whiskers (Fig. 3 and Fig. 5) justified this fact. Summer is dominated by unpredictable small-scale convective cells (Beck et al., 2019; Tapiador et al., 2020). Representation of these convective precipitation is still a limitation of the current reanalysis as reported by Ebert et al. (2007), de Leeuw et al. (2015), Acharya et al. (2019), Xin et al. (2021) amongst others. In relation with this fact, overestimation is generally observed during these months, which has been also reported in Jiao et al. (2021) and Longo-Minnolo et al. (2022).

The pdf assessment revealed that ERA5/ERA5-Land generally reproduced the spatial location of precipitation frequency but disagrees in terms of magnitude. It tends to underestimate the no-precipitation, heavy and violent categories while overestimating light and moderate precipitation. This finding agrees with studies that highlighted a general overestimation of precipitation frequency in reanalysis (Beck et al., 2017; Hénin et al., 2018) and an underestimation of heavy precipitation events (Crossett et al., 2020; Jiang et al., 2021; Bližňák et al., 2022). The eps-singleton test highlighted the N, NE and SE regions as the most deviated from AEMET probability distribution. These areas are of special difficulty for the reanalysis because of the complex topography, the closeness to the coast and the predominant role of convection in the precipitation formation, especially for the eastern coast.

6.1.2. Spatial and temporal assessment

ECMWF reanalysis was found to reproduce the pattern of daily and monthly precipitation for the country (Fig. 9) being able to capture the most part of the spatio-temporal variance. Similar good performance was obtained from an EOF analysis in Jiao et al. (2021) for China. ECMWF first and second EOFs mostly reproduce the AEMET EOFs spatial pattern, with discrepancies occurring in the third EOF. Nevertheless, AEMET displays enhanced spatial features in comparison to the reanalysis, especially over mountain regions (the Central System, Sierra Morena mountains near the Guadalquivir depression). This fact highlights the reanalysis difficulty in properly capturing the spatio-temporal variance of areas with complex topography (Amjad et al., 2020; Jiao et al., 2021). SPAEF values generally confirm the good representation of the precipitation spatial patterns. Worse performance is observed at daily scale (shift in the median and wider boxes and whiskers) mainly due to the higher level of variability at this temporal scale.

Using reanalysis for temporal trend assessment remains challenging due to the spurious variability that could be introduced in the output signal because of the temporally fluctuating number of observations and biases in assimilated observations and models (Bengtsson et al., 2004; Thorne and Vose, 2010). However, reanalysis have been often used, especially when no alternative source of data existed (Lindsay et al., 2014). Recent applications of ECMWF precipitation trend analysis can be found in Chiaravalloti et al. (2022) and Varlas et al. (2022). Gridded observations can be affected also by the temporal variability of the network (Herrera et al., 2016). Despite the possible associated uncertainties, the temporal trend assessment revealed that ECMWF reanalysis generally reproduced AEMET annual and seasonal temporal trends (Fig. 10). SON provided the most discrepant behaviour displaying an overestimation of positive trend values. Discrepancies also existed in the total extent of the spatial features observed (Fig. 10a). Reanalysis indicated no significative precipitation trend (Fig. S14-S16). Although a strict comparison with studies compiled from scientific literature is not straightforward, mainly due to differences in the times series considered (i.e., time period, number of stations, precise location and spatial distribution of the stations, etc), the generalized dominant negative annual trend is also documented in Ruiz Sinoga et al. (2011) for the region of Andalusia, Del Río et al. (2005) for Castille and Leon region, and De Luis et al. (2009) for the Mediterranean region. Río et al. (2011) documented

significant decreases in > 28% of Spain in summer and winter. Positive trends were reported in De Luis et al. (2009) and Fernández-Montes and Rodrigo (2015) for locations in the eastern and southern eastern coast at annual scale and especially for the winter season.

6.1.3. Error dependency with precipitation-intensity and topography

The continuous and categorical analysis under different precipitation intensities reported a deteriorated performance for the heavy and violent categories (Fig. 11) (greater variability and deteriorated metric values). For ERA5, Jiang et al. (2021) and Xin et al. (2021) documented a similar RMSE increase and progressive change from overestimation to underestimation with precipitation intensity over China. Moderate category displayed the best KGE performance (Fig. 11d) and better precipitation event discrimination than the rest of the categories (Fig. 11e-f), in exception of NP. This is because of the dry days misclassification issue in LP and the underestimation of HP and VP. For ERA5, better precipitation discrimination for this category was also reported in Hafizi and Sorman (2022) and Kolluru et al. (2020). Similar behaviour was obtained over Australia for ERA-Interim as documented in Acharya et al. (2019). No precipitation category has a proper detection but only assigns a small portion of the ground-truth no-precipitation events. The events missed however increase the resulting overestimation (Fig. 11b) and deteriorated performance (Fig. 11d).

The error analysis with orography revealed that model estimation and detection capability generally deteriorate in areas with more complex topography (Fig. 11a-f). General significant correlation for the different climatic regions supports this fact (Table 4). Orographic dependence was also easily deductible in Fig. 2. Difficulties in the provision of high-quality precipitation reanalysis estimates in mountainous terrain were also reported in previous studies (Beck et al., 2019; Amjad et al., 2020; Chen et al., 2021; Jiao et al., 2021; Longo-Minnolo et al., 2022). A clearer relationship is obtained for the slope than elevation itself (Fig. 11a-f) (in exception of the kappa statistic). In fact, the turning point in RMSE (Fig. 13c) can be attributed to the general flat conditions of the Meseta region (between 600 and 800 m.a.s.l). Amjad et al. (2020) highlighted a deviation in climatological totals with slope. Longo-Minnolo et al. (2022) reported significant correlation between altitude variation within each ERA5-Land cell and RMSE. This within-cell altitude variation can be easily linked with the slope. KGE performance, contrary to the rest of the statistics, did not reveal a strong correlation with elevation or slope. This is mainly due to the disparity observed amongst the climatic regions considered.

6.1.4. Differences between ERA5/ERA5-Land

ERA5-Land and ERA5 performed very similar as it was expected (ERA-5 Land is a rerun of ERA-5). Similar performance was reproduced for all the analysis and only minor discrepancies were obtained for the absolute values of the metrics (slightly higher temporal variability for ERA5-Land). Similar findings were indicated by Xin et al. (2021), Chen et al. (2021) and Bližňák et al. (2022). Although the ERA5-Land higher spatial resolution could be useful in regions with complex topography, no added improvement is obtained regarding orographically induced precipitation (Zandler et al., 2019; Hamm et al., 2020).

6.2. Future improvements

This study has highlighted some weaknesses of the ECMWF precipitation product. To be strictly fair, it should be stressed that the approach considered suffers from a limitation present in many studies: the uncertainty associated with the observations. Quality of the spatially interpolated products is highly dependent on the network density, homogeneity, quality control, interpolation algorithms, orographical conditions (Peral García et al., 2017; Herrera et al., 2019). However, these limitations have been considered, as far as possible, in the generation of the AEMET product (Peral García et al., 2017). In addition, using high-resolution gridded datasets as reference for product evaluation has also been undertaken in Beck et al. (2019), Tapiador et al. (2020), Bandhauer et al. (2022) amongst others. Grid-to-point analysis is also not free from associated uncertainties due to scale mismatch and representativeness (Amjad et al., 2020). In any case, this study can evaluate how well the test dataset satisfy a common user expectation (i.e., what could be the discrepancies when using ECMWF's reanalysis precipitation product instead of the reference Spanish Meteorological Agency provided dataset).

Focusing on the study region, despite the extensive assessment of the ECMWF precipitation performed in this study there are still open questions to contribute: satellite performance vs. reanalysis performance (partly introduced in Tapiador et al. (2020)), evaluation under a hydrological framework (as in Senent-Aparicio et al., 2018), assessment of extremes (based on Hénin et al. (2018)), assessment using new tools such as Triple Collocation Analysis (TCA) (Li et al., 2018), sub-daily assessment, amongst others.

7. Conclusions

This study provides a detailed evaluation of latest fifth generation of ECMWF's precipitation products over Spain. The results obtained here contribute to fill the knowledge gap refering to the performance of the new ERA5-Land/ERA5 precipitation products over Spain and over the Mediterranean region and thus contributing to the global evaluation of these products that is being performed globally. The reanalysis precipitation evaluation was based on a comparison with Spanish National Meteorological Agency long time series (1951–2020) observed gridded product. The results obtained here are consistent with finding with previous studies. The following main conclusions were drawn from the study:

- Continuous assessment revealed a general good agreement between both observed and reanalysis datasets: spearman correlation (0.5–0.9),RMSE (mostly between 2 and 8 mm/d) and KGE values > 0.4. Worst continuous performance was obtained in summer months, with a generalized overestimation.
- Categorical assessment indicated a generalized good precipitation detection (kappa values between 0.4 and 0.8) confirmed by the chi-square statistics. A wet bias was revealed especially over the eastern coast, as indicated by the decrease/increase in POD/FAR. Worst performance was obtained during summer months.
- PDF assessment indicated that ERA5-Land/ERA5 tended to overestimate light (≥1 and < 5 mm/day), and moderate (≥5 and < 20 mm/day) precipitation categories while underestimating the heavy (≥20 and < 40 mm/day) and violent (≥40 mm/day) categories. Mediterranean and northern coast were highlighted as the most pdf discrepant, as shown by the Epps-Singleton test.
- Spatial and temporal pattern assessment showed a good agreement between the spatial patterns and temporal trends of the observed and reanalysis datasets.
- Error dependency on precipitation intensity and orography highlighted moderate category had the best model performance. Precipitation estimation and detection were found to be dependent on orography. Positive correlations were obtained for RBIAS (0.41/0.35, for ERA5-Land/ERA5) and RMSE (0.69/0.70) while negative correlation was found for Kappa (−0.29/−0.34).
- No significant differences were deduced between the ERA5-Land and ERA5 results as indicated by the different analysis performed.

Conclusions provided by this study could be useful for hydrological and meteorological applications that make use of these precipitation datasets over the region.

CRediT authorship contribution statement

José Gomis-Cebolla: Conceptualization, Methodology, Formal

analysis, Writing – original draft, Writing – review & editing. **Viera Rattayova:** Methodology, Formal analysis, Writing – original draft, Writing – review & editing. **Sergio Salazar-Galán:** Formal analysis, Resources, Writing – review & editing. **Félix Francés:** Supervision, Project administration, Funding acquisition, Writing – review & editing.

Declaration of Competing Interest

The authors declare that they have no known competing financial interests or personal relationships that could have appeared to influence the work reported in this paper.

Data availability

Data will be made available on request.

Acknowledgments

This study was founded by the Spanish AEI within the program WaterJPI through the project iAqueduct (PCI2019-103729), and by the project Water4Cast funded by Generalitat Valenciana (PROMETEO/2021/074). The author thanks AEMET for the data provided for this work (AEMET dataset available at http://www.aemet.es/va/serviciosclimaticos/cambio_climat/datos_diarios?w=2&w2=0. ECMWF reanalysis is also acknowledged for ERA5 and ERA5-Land data available from the Copernicus climate data store (https://cds.climate.copernicus.eu/). Datasets were accessed on 21th January 2022.

Appendix A. Supplementary data

Supplementary data to this article can be found online at https://doi.org/10.1016/j.atmosres.2023.106606.

References

Acharya, S.C., Nathan, R., Wang, Q.J., Su, C.H., Eizenberg, N., 2019. An evaluation of daily precipitation from a regional atmospheric reanalysis over Australia. Hydrol. Earth Syst. Sci. 23, 3387–3403. https://doi.org/10.5194/hess-23-3387-2019.

Amjad, M., Yilmaz, M.T., Yucel, I., Yilmaz, K.K., 2020. Performance evaluation of satellite- and model-based precipitation products over varying climate and complex topography. J. Hydrol. (Amst) 584, 124707. https://doi.org/10.1016/j.jhydrol.2020.124707.

Bandhauer, M., Isotta, F., Lakatos, M., Lussana, C., Båserud, L., Izsák, B., Szentes, O., Tveito, O.E., Frei, C., 2022. Evaluation of daily precipitation analyses in E-OBS (v19.0e) and ERA5 by comparison to regional high-resolution datasets in European regions. Int. J. Climatol. 42, 727–747. https://doi.org/10.1002/joc.7269.

Beck, H.E., Vergopolan, N., Pan, M., Levizzani, V., van Dijk, A.I.J.M., Weedon, G.P., Brocca, L., Pappenberger, F., Huffman, G.J., Wood, E.F., 2017. Global-scale evaluation of 22 precipitation datasets using gauge observations and hydrological modeling. Hydrol. Earth Syst. Sci. 21, 6201–6217. https://doi.org/10.5194/hess-21-6201-2017.

Beck, H.E., Pan, M., Roy, T., Weedon, G.P., Pappenberger, F., van Dijk, A.I.J.M., Huffman, G.J., Adler, R.F., Wood, E.F., 2019. Daily evaluation of 26 precipitation datasets using Stage-IV gauge-radar data for the CONUS. Hydrol. Earth Syst. Sci. 23, 207–224. https://doi.org/10.5194/hess-23-207-2019.

Belo-Pereira, M., Dutra, E., Viterbo, P., 2011. Evaluation of global precipitation data sets over the Iberian Peninsula. J. Geophys. Res.-Atmos. 116 https://doi.org/10.1029/2010JD015481.

Bengtsson, L., Hagemann, S., Hodges, K.I., 2004. Can climate trends be calculated from reanalysis data? J. Geophys. Res. D Atmos. 109, 1–8. https://doi.org/10.1029/2004JD004536.

Bližňák, V., Pokorná, L., Rulfová, Z., 2022. Assessment of the capability of modern reanalyses to simulate precipitation in warm months using adjusted radar precipitation. J. Hydrol. Reg. Stud. 42, 101121. https://doi.org/10.1016/j.ejrh.2022.101121.

Bosilovich, M.G., Chen, J., Robertson, F.R., Adler, R.F., 2008. Evaluation of global precipitation in reanalyses. J. Appl. Meteorol. Climatol. 47 (9), 2279–2299. https://doi.org/10.1175/2008JAMC1921.1.

Caracciolo, D., Francipane, A., Viola, F., Noto, L.V., Deidda, R., 2018. Performances of GPM satellite precipitation over the two major Mediterranean islands. Atmos. Res. 213, 309–322. https://doi.org/10.1016/j.atmosres.2018.06.010.

Chen, H., Yong, B., Shen, Y., Liu, J., Hong, Y., Zhang, J., 2020. Comparison analysis of six purely satellite-derived global precipitation estimates. J. Hydrol. (Amst) 581, 124376. https://doi.org/10.1016/j.jhydrol.2019.124376.

Chen, Y., Sharma, S., Zhou, X., Yang, K., Li, X., Niu, X., Hu, X., Khadka, N., 2021. Spatial performance of multiple reanalysis precipitation datasets on the southern slope of central Himalaya. Atmos. Res. 250, 105365 https://doi.org/10.1016/j.atmosres.2020.105365.

Chiaravalloti, F., Caloiero, T., Coscarelli, R., 2022. The long-term ERA5 data series for trend analysis of rainfall in Italy. Hydrology (Basel) 9 (2), 18. https://doi.org/10.3390/hydrology9020018.

Cortesi, N., Gonzalez-Hidalgo, J.C., Trigo, R.M., Ramos, A.M., 2014. Weather types and spatial variability of precipitation in the Iberian Peninsula. Int. J. Climatol. 34, 2661–2677. https://doi.org/10.1002/joc.3866.

Crossett, C.C., Betts, A.K., Dupigny-Giroux, L.A.L., Bomblies, A., 2020. Evaluation of daily precipitation from the ERA5 global reanalysis against GHCN observations in the northeastern United States. Climate (Basel) 8 (12), 148. https://doi.org/10.3390/cli8120148.

de Castro, M., Martín-Vide, J., Alonso, S., Abaurrea, C.J., Asín, J., Barriendos, M., Brunet, M., Creus, J., Galán, E., Gaertner, M.A., Gallardo, C., González-Hidalgo, J.C., Guijarro, J.A., Luna, Y., Pozo-Vázquez, A.D., Quereda, J., Rodrigo, F.S., Rodríguez-Puebla, C., Rosell-Melé, A., Almarza, R.C., Zurita, E., 2005. El clima de España: pasado, presente y escenarios de clima para el siglo XXI.

de Leeuw, J., Methven, J., Blackburn, M., 2015. Evaluation of ERA-Interim reanalysis precipitation products using England and Wales observations. Q. J. R. Meteorol. Soc. 141, 798–806. https://doi.org/10.1002/qj.2395.

De Luis, M., González-Hidalgo, J.C., Longares, L.A., Štepánek, P., 2009. Seasonal precipitation trends in the Mediterranean Iberian Peninsula in second half of 20th century. Int. J. Climatol. 29 (9), 1312–1323. https://doi.org/10.1002/joc.1778.

Dee, D.P., Uppala, S.M., Simmons, A.J., Berrisford, P., Poli, P., Kobayashi, S., Andrae, U., Balmaseda, M.A., Balsamo, G., Bauer, P., Bechtold, P., Beljaars, A.C.M., van de Berg, L., Bidlot, J., Bormann, N., Delsol, C., Dragani, R., Fuentes, M., Geer, A.J., Haimberger, L., Healy, S.B., Hersbach, H., Hólm, E.V., Isaksen, L., Kållberg, P., Köhler, M., Matricardi, M., Mcnally, A.P., Monge-Sanz, B.M., Morcrette, J.J., Park, B.K., Peubey, C., de Rosnay, P., Tavolato, C., Thépaut, J.N., Vitart, F., 2011. The ERA-Interim reanalysis: configuration and performance of the data assimilation system. Q. J. R. Meteorol. Soc. 137, 553–597. https://doi.org/10.1002/qj.828.

Del Río, S., Penas, Á., Fraile, R., 2005. Analysis of recent climatic variations in Castile and Leon (Spain). Atmos. Res. 73 (1–2), 69–85. https://doi.org/10.1016/j.atmosres.2004.06.005.

Ebert, E.E., Janowiak, J.E., Kidd, C., 2007. Comparison of near-real-time precipitation estimates from satellite observations and numerical models. Bull. Am. Meteorol. Soc. 88, 47–64. https://doi.org/10.1175/BAMS-88-I-47.

Ebita, A., Kobayashi, S., Ota, Y., Moriya, M., Kumabe, R., Onogi, K., Harada, Y., Yasui, S., Miyaoka, K., Takahashi, K., Kamahori, H., Kobayashi, C., Endo, H., Soma, M., Oikawa, Y., Ishimizu, T., 2011. The Japanese 55-year reanalysis "JRA-55": an Interim Report. Sci. Online Lett. Atmos. 7, 149–152. https://doi.org/10.2151/sola.2011-038.

el Kenawy, A.M., Lopez-Moreno, J.I., McCabe, M.F., Vicente-Serrano, S.M., 2015. Evaluation of the TMPA-3B42 precipitation product using a high-density rain gauge network over complex terrain in northeastern Iberia. Glob. Planet. Chang. 133, 188–200. https://doi.org/10.1016/j.gloplacha.2015.08.013.

Epps, T.W., Singleton, K.J., 1986. An omnibus test for the two- sample problem using the empirical characteristic function. J. Stat. Comput. Simul. 26, 177–203. https://doi.org/10.1080/00949658608810963.

Fernández-Montes, S., Rodrigo, F.S., 2015. Trends in surface air temperatures, precipitation and combined indices in the southeastern Iberian Peninsula (1970-2007). Clim. Res. 63 (1), 43–60. https://doi.org/10.3354/cr01287.

Gelaro, R., McCarty, W., Suárez, M.J., Todling, R., Molod, A., Takacs, L., Randles, C.A., Darmenov, A., Bosilovich, M.G., Reichle, R., Wargan, K., Coy, L., Cullather, R., Draper, C., Akella, S., Buchard, V., Conaty, A., da Silva, A.M., Gu, W., Kim, G.K., Koster, R., Lucchesi, R., Merkova, D., Nielsen, J.E., Partyka, G., Pawson, S., Putman, W., Rienecker, M., Schubert, S.D., Sienkiewicz, M., Zhao, B., 2017. The modern-era retrospective analysis for research and applications, version 2 (MERRA-2). J. Clim. 30, 5419–5454. https://doi.org/10.1175/JCLI-D-16-0758.1.

Gibson, J.K., Kållberg, P., Uppala, S., Hernandez, A., Nomura, A., Serrano, E., 1999. ERA-15 Description. ECMWF Re-Analysis Project Report Series, 1.

Gleixner, S., Demissie, T., Diro, G.T., 2020. Did ERA5 improve temperature and precipitation reanalysis over East Africa? Atmosphere (Basel) 11, 1–19. https://doi.org/10.3390/atmos11090996.

Gomis-Cebolla, J., Garcia-Arias, A., Perpinyà-Vallès, M., Francés, F., 2022. Evaluation of Sentinel-1, SMAP and SMOS surface soil moisture products for distributed eco-hydrological modelling in Mediterranean forest basins. J. Hydrol. (Amst) 608. https://doi.org/10.1016/j.jhydrol.2022.127569.

Hafizi, H., Sorman, A.A., 2022. Assessment of 13 gridded precipitation datasets for hydrological modeling in a Mountainous Basin. Atmosphere (Basel) 13. https://doi.org/10.3390/atmos13010143.

Hallouin, T., 2021. hydroeval: An Evaluator for Streamflow Time Series in Python (Version 0.1.0). Zenodo. https://doi.org/10.5281/zenodo.2591217.

Hamed, K.H., 2009. Enhancing the effectiveness of prewhitening in trend analysis of hydrologic data. J. Hydrol. (Amst) 368. https://doi.org/10.1016/j.jhydrol.2009.01.040.

Hamm, A., Arndt, A., Kolbe, C., Wang, X., Thies, B., Boyko, O., Reggiani, P., Scherer, D., Bendix, J., Schneider, C., 2020. Intercomparison of gridded precipitation datasets over a sub-region of the central himalaya and the southwestern tibetan plateau. Water (Switzerland) 12. https://doi.org/10.3390/w12113271.

He, X., Pan, M., Wei, Z., Wood, E.F., Sheffield, J., 2020. A global drought and flood catalogue from 1950 to 2016. Bull. Am. Meteorol. Soc. 101, E508–E535. https://doi.org/10.1175/BAMS-D-18-0269.1.

Hénin, R., Liberato, M.L.R., Ramos, A.M., Gouveia, C.M., 2018. Assessing the use of satellite-based estimates and high-resolution precipitation datasets for the study of extreme precipitation events over the Iberian Peninsula. Water (Switzerland) 10. https://doi.org/10.3390/w10111688.

Herrera, S., Fernández, J., Gutiérrez, J.M., 2016. Update of the Spain02 gridded observational dataset for EURO-CORDEX evaluation: Assessing the effect of the interpolation methodology. Int. J. Climatol. 36, 900–908. https://doi.org/10.1002/joc.4391.

Herrera, S., Margarida Cardoso, R., Matos Soares, P., Espírito-Santo, F., Viterbo, P., Gutiérrez, J.M., 2019. Iberia01: A new gridded dataset of daily precipitation and temperatures over Iberia. Earth Syst. Sci. Data 11, 1947–1956. https://doi.org/10.5194/essd-11-1947-2019.

Hersbach, H., Bell, B., Berrisford, P., Hirahara, S., Horányi, A., Muñoz-Sabater, J., Nicolas, J., Peubey, C., Radu, R., Schepers, D., Simmons, A., Soci, C., Abdalla, S., Abellan, X., Balsamo, G., Bechtold, P., Biavati, G., Bidlot, J., Bonavita, M., de Chiara, G., Dahlgren, P., Dee, D., Diamantakis, M., Dragani, R., Flemming, J., Forbes, R., Fuentes, M., Geer, A., Haimberger, L., Healy, S., Hogan, R.J., Hólm, E., Janisková, M., Keeley, S., Laloyaux, P., Lopez, P., Lupu, C., Radnoti, G., de Rosnay, P., Rozum, I., Vamborg, F., Villaume, S., Thépaut, J.N., 2020. The ERA5 global reanalysis. Q. J. R. Meteorol. Soc. 146, 1999–2049. https://doi.org/10.1002/qj.3803.

Hu, Q., Li, Z., Wang, L., Huang, Y., Wang, Y., Li, L., 2019. Rainfall spatial estimations: a review from spatial interpolation to multi-source data merging. Water (Switzerland). https://doi.org/10.3390/w11030579.

Jiang, Q., Li, W., Fan, Z., He, X., Sun, W., Chen, S., Wang, J., 2021. Evaluation of the ERA5 reanalysis precipitation dataset over Chinese Mainland. J. Hydrol. (Amst) 595. https://doi.org/10.1016/j.jhydrol.2020.125660.

Jiao, D., Xu, N., Yang, F., Xu, K., 2021. Evaluation of spatial-temporal variation performance of ERA5 precipitation data in China. Sci. Rep. 11, 1–13. https://doi.org/10.1038/s41598-021-97432-y.

Kalnay, E., Kanamitsu, M., Kistler, R., Collins, W., Deaven, D., Gandin, L., Iredell, M., Saha, S., White, G., Woollen, J., Zhu, Y., Chelliah, M., Ebisuzaki, W., Higgins, W., Janowiak, J., Mo, K.C., Ropelewski, C., Wang, J., Leetmaa, A., Reynolds, R., Jenne, R., Joseph, D., 1996. The NCEP/NCAR 40-Year Reanalysis Project.

Kanamitsu, M., Ebisuzaki, W., Woollen, J., Yang, S.-K., Hnilo, J.J., Fiorino, M., Potter, G. L., 2002. NCEP–DOE AMIP-II reanalysis (R-2). Bull. Am. Meteorol. Soc. 83, 1631–1644. https://doi.org/10.1175/BAMS-83-11-1631.

Koch, J., Demirel, M.C., Stisen, S., 2018. The SPAtial EFficiency metric (SPAEF): multiple-component evaluation of spatial patterns for optimization of hydrological models. Geosci. Model Dev. 11, 1873–1886. https://doi.org/10.5194/gmd-11-1873-2018.

Kolluru, V., Kolluru, S., Konkathi, P., 2020. Evaluation and integration of reanalysis rainfall products under contrasting climatic conditions in India. Atmos. Res. 246 https://doi.org/10.1016/j.atmosres.2020.105121.

Li, C., Tang, G., Hong, Y., 2018. Cross-evaluation of ground-based, multi-satellite and reanalysis precipitation products: applicability of the triple collocation method across Mainland China. J. Hydrol. (Amst) 562, 71–83. https://doi.org/10.1016/j.jhydrol.2018.04.039.

Lindsay, R., Wensnahan, M., Schweiger, A., Zhang, J., 2014. Evaluation of seven different atmospheric reanalysis products in the Arctic. J. Clim. 27 (7), 2588–2606. https://doi.org/10.1175/JCLI-D-13-00014.1.

Lockhoff, M., Zolina, O., Simmer, C., Schulz, J., 2019. Representation of precipitation characteristics and extremes in regional reanalyses and satellite-and gauge-based estimates over western and Central Europe. J. Hydrometeorol. 20, 1123–1145. https://doi.org/10.1175/JHM-D-18-0200.1.

Longo-Minnolo, G., Vanella, D., Consoli, S., Pappalardo, S., Ramírez-Cuesta, J.M., 2022. Assessing the use of ERA5-Land reanalysis and spatial interpolation methods for retrieving precipitation estimates at basin scale. Atmos. Res. 271, 106131 https://doi.org/10.1016/j.atmosres.2022.106131.

Manzano, A., Clemente, M.A., Morata, A., Luna, M.Y., Beguería, S., Vicente-Serrano, S. M., Martín, M.L., 2019. Analysis of the atmospheric circulation pattern effects over SPEI drought index in Spain. Atmos. Res. 230 https://doi.org/10.1016/j.atmosres.2019.104630.

Muñoz-Sabater, J., Dutra, E., Agustí-Panareda, A., Albergel, C., Arduini, G., Balsamo, G., Boussetta, S., Choulga, M., Harrigan, S., Hersbach, H., Martens, B., Miralles, D.G., Piles, M., Rodríguez-Fernández, N.J., Zsoter, E., Buontempo, C., Thépaut, J.N., 2021. ERA5-Land: a state-of-the-art global reanalysis dataset for land applications. Earth Syst. Sci. Data 13, 4349–4383. https://doi.org/10.5194/essd-13-4349-2021.

Navascués, B., Rodríguez, E., Ayuso, J.J., Järvenoja, S., 2003. Analysis of surface variables and parameterization of surface processes in HIRLAM. Part II: Seasonal assimilation experiment.

Nogueira, M., 2020. Inter-comparison of ERA-5, ERA-interim and GPCP rainfall over the last 40 years: process-based analysis of systematic and random differences. J. Hydrol. (Amst) 583, 124632. https://doi.org/10.1016/j.jhydrol.2020.124632.

Patakamuri, S.K., O'Brien, N., 2021. modifiedmk: Modified Versions of Mann Kendall and Spearman's Rho Trend Tests. R package version 1.6. https://CRAN.R-project.org/package=modifiedmk.

Peral García, C., Navascués Fernández-Victorio, B., Ramos Calzado, P., 2017. Serie de precipitación diaria en rejilla con fines climáticos. Serie de precipitación diaria en rejilla con fines climáticos. https://doi.org/10.31978/014-17-009-5.

Piao, S., Ciais, P., Huang, Y., Shen, Z., Peng, S., Li, J., Zhou, L., Liu, H., Ma, Y., Ding, Y., Friedlingstein, P., Liu, C., Tan, K., Yu, Y., Zhang, T., Fang, J., 2010. The impacts of climate change on water resources and agriculture in China. Nature 467, 43–51. https://doi.org/10.1038/nature09364.

Pool, S., Vis, M., Seibert, J., 2018. Evaluating model performance: towards a non-parametric variant of the Kling-Gupta efficiency. Hydrol. Sci. J. 63 https://doi.org/10.1080/02626667.2018.1552002.

Quintana-Seguí, P., Peral, C., Turco, M., Llasat, M.C., Martin, E., 2016. Meteorological analysis systems in North-East Spain: validation of SAFRAN and SPAN. J. Environ. Inf. 27, 116–130. https://doi.org/10.3808/jei.201600335.

Rienecker, M.M., Suarez, M.J., Gelaro, R., Todling, R., Bacmeister, J., Liu, E., Bosilovich, M.G., Schubert, S.D., Takacs, L., Kim, G., Bloom, S., Chen, J., Collins, D., Conaty, A., da Silva, A., Gu, W., Joiner, J., Koster, R.D., Lucchesi, R., Molod, A., Owens, T., Pawson, S., Pegion, P., Redder, C.R., Reichle, R., Robertson, F.R., Ruddick, A.G., Sienkiewicz, M., Woollen, J., 2011. MERRA: NASA's Modern-Era Retrospective Analysis for Research and Applications. J. Clim. 24 (14), 3624–3648. https://doi.org/10.1175/JCLI-D-11-00015.1.

Río, S.D., Herrero, L., Fraile, R., Penas, A., 2011. Spatial distribution of recent rainfall trends in Spain (1961–2006). Int. J. Climatol. 31 (5), 656–667. https://doi.org/10.1002/joc.2111.

Robertson, D.E., Shrestha, D.L., Wang, Q.J., 2013. Post-processing rainfall forecasts from numerical weather prediction models for short-term streamflow forecasting. Hydrol. Earth Syst. Sci. 17, 3587–3603. https://doi.org/10.5194/hess-17-3587-2013.

Rodríguez, E., Navascués, B., Ayuso, J.J., Järvenoja, S., 2003. Analysis of surface variables and parameterization of surface processes in HIRLAM. Part I: Approach and verification by parallel runs.

Ruiz Sinoga, J.D., Garcia Marin, R., Martinez Murillo, J.F., Gabarron Galeote, M.A., 2011. Precipitation dynamics in southern Spain: trends and cycles. Int. J. Climatol. 31 (15), 2281–2289. https://doi.org/10.1002/joc.2235.

Salazar-Galán, S., García-Bartual, R., Salinas, J.L., Francés, F., 2021. A process-based flood frequency analysis within a trivariate statistical framework. Application to a semi-arid Mediterranean case study. J. Hydrol. (Amst) 603. https://doi.org/10.1016/j.jhydrol.2021.127081.

Senent-Aparicio, J., López-Ballesteros, A., Pérez-Sánchez, J., Segura-Méndez, F.J., Pulido-Velazquez, D., 2018. Using multiple monthly water balance models to evaluate gridded precipitation products over peninsular Spain. Remote Sens. 10 https://doi.org/10.3390/rs10060922.

Senent-Aparicio, J., Jimeno-Sáez, P., López-Ballesteros, A., Giménez, J.G., Pérez-Sánchez, J., Cecilia, J.M., Srinivasan, R., 2021. Impacts of swat weather generator statistics from high-resolution datasets on monthly streamflow simulation over Peninsular Spain. J. Hydrol. Reg. Stud. 35 https://doi.org/10.1016/j.ejrh.2021.100826.

Serrano, A., García, J., Mateos, V.L., Cancillo, M.L., Garrido, J., 1999. Monthly modes of variation of precipitation over the Iberian Peninsula. J. Clim. 12, 2894–2919. https://doi.org/10.1175/1520-0442(1999)012<2894:MMOVOP>2.0.CO;2.

Sharifi, E., Eitzinger, J., Dorigo, W., 2019. Performance of the state-of-the-art gridded precipitation products over mountainous terrain: a regional study over Austria. Remote Sens. 11 https://doi.org/10.3390/rs11172018.

Sun, Q., Miao, C., Duan, Q., Ashouri, H., Sorooshian, S., Hsu, K.L., 2018. A review of global precipitation data sets: data sources, estimation, and intercomparisons. Rev. Geophys. 56, 79–107. https://doi.org/10.1002/2017RG000574.

Tang, G., Clark, M.P., Papalexiou, S.M., Ma, Z., Hong, Y., 2020. Have satellite precipitation products improved over last two decades? A comprehensive comparison of GPM IMERG with nine satellite and reanalysis datasets. Remote Sens. Environ. 240 https://doi.org/10.1016/j.rse.2020.111697.

Tapiador, F.J., Turk, F.J., Petersen, W., Hou, A.Y., García-Ortega, E., Machado, L.A.T., Angelis, C.F., Salio, P., Kidd, C., Huffman, G.J., de Castro, M., 2012. Global precipitation measurement: methods, datasets and applications. Atmos. Res. 104–105, 70–97. https://doi.org/10.1016/j.atmosres.2011.10.021.

Tapiador, F.J., Navarro, A., García-Ortega, E., Merino, A., Sánchez, J.L., Marcos, C., Kummerow, C., 2020. The contribution of rain gauges in the calibration of the IMERG product: results from the first validation over Spain. J. Hydrometeorol. 21, 161–182. https://doi.org/10.1175/JHM-D-19-0116.1.

Tarek, M., Brissette, F.P., Arsenault, R., 2020. Evaluation of the ERA5 reanalysis as a potential reference dataset for hydrological modelling over North America. Hydrol. Earth Syst. Sci. 24, 2527–2544. https://doi.org/10.5194/hess-24-2527-2020.

Thorne, P.W., Vose, R.S., 2010. Reanalyses suitable for characterizing long-term trends. Bull. Am. Meteorol. Soc. 91, 353–362. https://doi.org/10.1175/2009BAMS2858.1.

Uppala, S.M., Kållberg, P.W., Simmons, A.J., Andrae, U., da Costa Bechtold, V., Fiorino, M., Gibson, J.K., Haseler, J., Hernandez, A., Kelly, G.A., Li, X., Onogi, K., Saarinen, S., Sokka, N., Allan, R.P., Andersson, E., Arpe, K., Balmaseda, M.A., Beljaars, A.C.M., van de Berg, L., Bidlot, J., Bormann, N., Caires, S., Chevallier, F., Dethof, A., Dragosavac, M., Fisher, M., Fuentes, M., Hagemann, S., Hólm, E., Hoskins, B.J., Isaksen, L., Janssen, P.A.E.M., Jenne, R., McNally, A.P., Mahfouf, J.F., Morcrette, J.J., Rayner, N.A., Saunders, R.W., Simon, P., Sterl, A., Trenberth, K.E., Untch, A., Vasiljevic, D., Viterbo, P., Woollen, J., 2005. The ERA-40 re-analysis. Q. J. R. Meteorol. Soc. https://doi.org/10.1256/qj.04.176.

Varlas, G., Stefanidis, K., Papaioannou, G., Panagopoulos, Y., Pytharoulis, I., Katsafados, P., Papadopoulos, A., Dimitriou, E., 2022. Unravelling precipitation trends in Greece since 1950s using ERA5 climate reanalysis data. Climate (Basel) 10 (2), 12. https://doi.org/10.3390/cli10020012.

Wang, C., Graham, R.M., Wang, K., Gerland, S., Granskog, M.A., 2019. Comparison of ERA5 and ERA-interim near-surface air temperature, snowfall and precipitation over Arctic Sea ice: effects on sea ice thermodynamics and evolution. Cryosphere 13, 1661–1679. https://doi.org/10.5194/tc-13-1661-2019.

Xin, Y., Lu, N., Jiang, H., Liu, Y., Yao, L., 2021. Performance of ERA5 reanalysis precipitation products in the Guangdong-Hong Kong-Macao greater Bay Area, China. J. Hydrol. (Amst) 602, 126791. https://doi.org/10.1016/j.jhydrol.2021.126791.

Xu, J., Ma, Z., Yan, S., Peng, J., 2022. Do ERA5 and ERA5-land precipitation estimates outperform satellite-based precipitation products? A comprehensive comparison

between state-of-the-art model-based and satellite-based precipitation products over mainland China. J. Hydrol. (Amst) 605. https://doi.org/10.1016/j.jhydrol.2021.127353.

Yue, S., Wang, C.Y., 2002. Applicability of prewhitening to eliminate the influence of serial correlation on the Mann-Kendall test. Water Resour. Res. 38 https://doi.org/10.1029/2001WR000861.

Zandler, H., Haag, I., Samimi, C., 2019. Evaluation needs and temporal performance differences of gridded precipitation products in peripheral mountain regions. Sci. Rep. 9 https://doi.org/10.1038/s41598-019-51666-z.